University of Oslo,
Department of Geosciences

Master Thesis

Drought in Greece under future climates

Author :
Anastasios G. Moukos

Supervisors:
Lena M. Tallaksen
James H. Stagge

A thesis submitted in fulfilment of the requirements
for the Greek-French program of postgraduate studies

"Management of Hydrometeorological Hazards-Hydrohasards"

in the

Laboratory of Hydrology and Aquatic Systems Analysis of the University of Thessaly (Department of Civil Engineering)

Laboratoire d' Etude des Transferts en Hydrologie et Environement of Observatoire des Sciences de l'Univers de Grenoble (OSUG) of Université Joseph Fourier – Grenoble I,

January 2015

Abstract

Drought is a major weather-related catastrophe worldwide that threatens sustainability of the global environment and human life. Under the general context of Global Climate Change the frequency and extent of droughts occurrence in the future are quite uncertain. The main goal of this thesis is to investigate how droughts will evolve in the 21st Century (2001-2100) in the wider area of Greece. To deal with the challenging issue to predict future changes in the evolution of drought hazard the widely used Standardized Precipitation Index (SPI) and the Standardized Precipitation-Evapotranspiration Index (SPEI) are elaborated. Both indices are calculated in similar manner. The basic difference is that the SPI is based on the precipitation values, while the SPEI is based on the simple water balance relationship defined by the difference between the precipitation and the evapotranspiration. Both indices are generated so for the control period of 1961-1990, as well as for the future period of 2001-2100. For the control period, the drought indices are produced following the original procedure. Though, another technique is adapted for the calculation of the indices for the future period. This technique uses the results of the control period as an input to estimate the drought indices values for the future period. The primary purpose of this method is to make the indices values of the historic and future period comparable. Moreover, the original procedure for the calculation of both indices is modified to achieve more accurate and more representative estimates for the certain study area. The database for this study is provided from the Water and Global Change (WATCH) project funded by the 6th Framework Programme (FP6) of European Research. Especially, it consists of the simulations of three General Circulation Models (GCM): The CNCM3, the ECHAM and the IPSL. The data are available for the control period as well as for two future climate scenarios, B1 and A2. The results of the present analysis indicate that the future climate of Greece is getting drier through the 21st Century. Although the difference is not so clear for the period between 2011-2040, it is highlighted that the droughts conditions of the 2041-2070 period, will be more extreme and with higher frequency than the ones of the control period. Finally, the results denote that the majority of the 2071-2100 years will be under extreme droughts in comparison with the reference period. Even if the resulted evolution of drought varies depending on the several GCMs and scenarios, all of the combinations of them confirm the increased drought occurrence in the future. Though, the results between the B1 and A2 scenarios present interesting differences. Especially, the former shows lower deviations from the control period droughts conditions than the latter. Additionally, SPEI drought index presents higher deviation from the control periods than the SPI index. Despite the differences caused by the drought index and the future climate scenario selected for the analysis, respectively, the final conclusions of the current thesis argue that the future climate of Greece will be significant drier than the historic period.

Περίληψη

Η ξηρασία είναι μία πολύ σημαντική φυσική καταστροφή παγκοσμίως, η οποία απειλεί την βιωσιμότητα του περιβάλλοντος και την ανθρώπινη ζωή. Σύμφωνα με το γενικό πλαίσιο της Παγκόσμιας Κλιματικής Αλλαγής η συχνότητα και η παράταση της εμφάνισης ξηρασίας στο μέλλον είναι πολύ αβέβαιη. Ο κύριος σκοπός της παρούσας μεταπτυχιακής εργασίας είναι να ερευνήσει πώς οι ξηρασίες θα εξελιχθούν στον 21ο Αιώνα (2001-2100) στην ευρύτερη περιοχή της Ελλάδος. Για την επίτευξη αυτής της πρόκλησης, της πρόβλεψης μελλοντικών αλλαγών του κινδύνου της ξηρασίας, οι ευρέως χρησιμοποιούμενοι Standardized Precipitation Index (SPI) και Standardized Precipitation-Evapotranspiration Index δείκτες ξηρασίας αναπαράχθηκαν. Και οι δύο δείκτες υπολογίζονται με παρόμοιο τρόπο. Η βασική διαφορά του είναι ότι ο SPI βασίζεται σε τιμές βροχόπτωσης, ενώ ο SPEI βασίζεται στο απλό υδάτινο ισοζύγιο που ορίζεται ως η διαφορά μεταξύ της βροχόπτωσης και της δυνητικής εξατμισοδιαπνοής. Και οι δύο δείκτες αναπαράγονται τόσο για την περίοδο αναφοράς 1961-1990, όσο για τη μελλοντική περίοδο 2001-2100. Για την περίοδο αναφοράς οι δείκτες ξηρασίας παράγονται ακολουθώντας την αρχική τους μεθοδολογία. Ενώ, άλλη τεχνική υιοθετείται για τον υπολογισμό των δεικτών για την μελλοντική περίοδο. Αυτή η τεχνική χρησιμοποιεί τα αποτελέσματα της περιόδου αναφοράς ως δεδομένα για να εκτιμηθούν οι τιμές των δεικτών ξηρασίας στη μελλοντική περίοδο. Ο βασικός σκοπός αυτής της μεθόδου είναι να κάνει τις τιμές των δεικτών για την ιστορική και τη μελλοντική περίοδο συγκρίσιμους. Επιπλέον, Η αρχική μεθοδολογία για τον υπολογισμό και των δύο δεικτών τροποποιείται για να επιτευχθεί μεγαλύτερη ακρίβεια και πιο αντιπροσωπευτικές εκτιμήσεις για την συγκεκριμένη περιοχή μελέτης. Η βάση δεδομένων για αυτή την μελέτη παρέχεται από το ερευνητικό σχέδιο Water and Global Change (WATCH) που υποστηρίχθηκε από το 6th Framework Programme (FP6) of European Research. Συγκεκριμένα, απαρτίζεται από τις προσομοιωμένες τιμές τριών Μοντέλων Γενικής Κυκλοφορίας (GCM): το CNCM3, το ECHAM και το IPSL. Δεδομένα είναι διαθέσιμα τόσο για τη περίοδο αναφοράς όσο και δύο μελλοντικά κλιματικά σενάρια, B1 και A2. Τα αποτελέσματα της παρούσας ανάλυσης δείχνουν ότι το μελλοντικό κλίμα της Ελλάδος τείνει να γίνεται όλο και πιο ξηρό κατά τον 21ο Αιώνα. Παρότι οι διαφορές δεν είναι τόσο ευδιάκριτες για την περίοδο 2011-2040, σημειώνεται ότι οι συνθήκες ξηρασίας της περιόδου 2041-2070, θα είναι πιο ακραίες και με μεγαλύτερη συχνότητα σε σχέση με την περίοδο αναφοράς. Τελικά, τα αποτελέσματα δηλώνουν ότι το μεγαλύτερο μέρος της χρονικής περιόδου 2071-2100 θα είναι υπό συνθήκες ακραίας ξηρασίας σε σχέση με την ιστορική περίοδο. Αν και η προκύπτουσα εξέλιξη των ξηρασιών ποικίλει όσον αφορά τα διάφορα GCMs και σενάρια, όλοι οι συνδυασμοί τους επιβεβαιώνουν την αυξανόμενη εμφάνιση ξηρασιών στο μέλλον. Παρόλα αυτά, τα αποτελέσματα μεταξύ των B1 και A2 σεναρίων παρουσιάζουν ενδιαφέρον διαφορές. Ειδικότερα, το πρώτο παρουσιάζει μικρότερες αποκλίσεις από την συνθήκες ξηρασίας της περίοδο αναφοράς από ότι το δεύτερο. Επιπροσθέτως, ο SPEI δείκτης ξηρασίας παρουσιάζει μεγαλύτερες αποκλίσεις σε σχέση με την περίοδο αναφοράς από τον δείκτη SPEI. Παρά τις διαφορές που προκύπτουν μεταξύ των δύο δεικτών και των επιλεγμένων μελλοντικών κλιματικών σεναρίων για αυτήν την ανάλυση, αντίστοιχα, το τελικό συμπέρασμα της συγκεκριμένης μεταπτυχιακής εργασίας είναι ότι το μελλοντικό κλίμα της Ελλάδος θα είναι σημαντικά ξηρότερο αναφορικά με την ιστορική περίοδο.

Acknowledgment:

I would like to thank Professor Lena Tallaksen and Postdoctoral Researcher James Stagge for creating and entrusting this subject to me and for the invaluable help and guidance they provided throughout the study.

Table of contents

1 Introduction

1.1 Drought in Greece

Drought is an extreme weather-related hazard with local to global scale consequences on the environment and the socio-economic life of the societies. The deficiency of a region in its water supply, whether atmospheric, surface or ground water leads to extremely inconvenient living conditions in both undeveloped and developed countries that are not properly prepared for this disruption. Impacts can refer to economic (e.g., crops destroy), environmental (e.g., losses or destruction of fish and wildlife habitat) or social (e.g., health problems related to low water flows and poor water quality) losses threatening the human life1.

In this study we use as study area Greece; a country suffering from water scarcity and the related impacts on agriculture and ecosystems. The causes of this scarcity could be categorized in two main classes. The primary one consists of the climate conditions and the subsequent frequent occurrence of droughts in both the dry and the wet seasons. The second category includes the mean administration of the reduced water sources for water supply, irrigation and drainage. Obviously, both climate change and the past unsustainable governmental policies are the precursors of the water sources reduction in the country. The pre-mentioned facts, in combination with the lack of a wide developed emergency system for droughts for the whole country, enhance the need for investigation of the droughts in future climates. For this reasons, the present work and other similar initiatives, seek to support new policies that could improve the present condition and ensure a future with less uncertainty.

The existing literature (scientific reports, journals and newspapers) indicates that Greece has been affected from droughts frequently in the past (Table 1). The impacts of droughts present significant diversity and most of the times great financial losses. Table 1 shows a subset of recorded drought events in the study area (see Annex A). The drought impacts are classified and recorded according to the European Drought Impact Inventory (EDII). Taking into account the results of this search and the existing entries from the European Drought Impact Inventory (EDII), it is obvious that Greece is affected from the majority of the impacts categories. The most frequent impacts are on: agriculture and livestock farming, forestry, water supply/water industries, water quality, human health, soil system, wildfires and

[1] http://drought.unl.edu/droughtforkids/howdoesdroughtaffectourlives/typesofdroughtimpacts.aspx

terrestrial ecosystems (habitats, plants and wildfire). The full classification of the several drought impacts is detailed extensively in Annex B.

Table 1: Sample of the drought impacts in Greece according to literature research for the purpose of the present work.

Drought Event	Country	Start date	End Date	Impact	Impact category	Impact description	NUTS 1	NUTS 2	NUTS 3
1999-2001	Greece	09/08/2001		7.1	Local water supply shortage/problems - drying up of local springs/wells	Danger of complete drying up of the local springs. Shortage of groundwater for agriculture use due to overexploitation from the drillings.	Kentriki Ellada	Voiotia	Orcho-menos
2000-2002	Greece	2000	2002	2.5	Increased dieback of trees (please specify tree species in the description field!)	3.5%, 4.9% & 5.9% of dead firs the years of 2000, 2001 & 2002, respectively.	Kentriki Ellada	Anatoliki Attiki	Parnitha
2007	Greece	Jul-07	Jul-07	4.1	Reduced hydropower production.	A week with frequent power cuts at several region of the country.	Ellada		
2007	Greece	Oct-07		8.8	Problems with drinking water quality	Deterioration of the taste and the smell of the drinking water, but no with the microbial load.	Kentriki Ellada	Thessalia	Karditsa
2007	Greece	Oct-07		10.1	Increased species mortality (specify species (latin term) and state whether a rare / endangered / protected species is concerned	50 member of the endangered species Capra aegagrus cretica, of a total population of 700 members, died while the rest survived after human action.	Nisia Aigaiou	Kyklades	Antimilos, island
2008	Greece	Aug-08		11.2	Structural damage to private property due to soil subsidence/shrinkage	Gaps in houses due to the prolonged drought	Voreia Ellada	Thessalia	Pinios, river
1958	Greece	20/08/1958	26/08/1958	14.3	Excess mortality during heat waves.	A heat wave of 7 days in Larissa and Trikala cost the life of about 600 people.	Voreia Ellada	Thessalia	Larissa and Trikala
2007	Greece	May-07	Aug-07	12.4	Other	A combination of increased area, and increased wildfires in number and severity. About 2.700 km2 burned area, at least 63 fatalities, 1500 burned houses, 6000 homeless, 5 billions damages, 4.5 millions	Ellada		

						olives trees and 60000 stock burned.			

1.2 Definition of drought

Before starting the presentation, it would be beneficial to give a definition of drought according to the existing literature. So, a drought could be defined as a sustained and regional occurrence of below average natural water availability (Tallaksen and Van Lanen, 2004), e.g. a period of (unusual) dry weather that persists long enough to cause problems such as crop damage and/or water supply shortages. The definition of Tallaksen and Van Lanen, (2004) implies that a drought can occur in any climate or region on Earth. A drought varies in spatial and temporal distribution, so an extreme spatial and/or temporal distributed event in combination with high severity and/or intensity is able to last months or years in continental scale. That could cause tremendous damage to economy and ecology and, in the worst case, bear enormous risks for life. In other words, drought belong to the most dangerous natural hazards. Europe has suffered from extreme drought events in the past, the time periods of 1962-64, 1975-76 and 1995-97 (Parry et al., 2012).Of course, a drought is able to be harmful in a local scale, but it wander from the aim of this work. This work, as part of a wider study for droughts in Europe, focuses on Greece area.

1.3 Classification of droughts

A retrospective on the existing literature regarding to the several kind of droughts is done before the exposition of the present thesis. As it mentioned in the review paper of Mishra, 2010, four categories of droughts have been identified (Wilhite and Glantz, 1985; American Meteorological Society, 2004). Meteorological drought, as a lack of precipitation over a region for a period of time, hydrological drought, which is related to a period with inadequate surface and subsurface water resources for established water uses of a given water resources management system, agricultural drought, which is defined as a period with declining soil moisture and consequent crop failure without any reference to surface water resources and, finally, the socio-economic drought, which is associated with the failure of water resources systems to meet water demands and thus associating droughts with supply of and demand for an economic good (water) (AMS, 2004). The same author, in the same work, underlines the need for research on the groundwater drought which refers to the occurrence and propagation of droughts in groundwater.

1.4 Investigation of past droughts

Scientists have done a lot of trials to investigate all the kinds of droughts so at the present (e.g. monitoring of droughts) as in the past and future. As the present work concerns the region of Europe and ,especially, in Greece, the studies of interest concentrate mainly to this part of the earth. Many scientists have approached the past droughts in Europe with several techniques. For example Stahl et al. (2010) investigated the trends in droughts in several regions of Europe for the period 1962-2004. Hannaford et al. (2013) illuminated the interdecadal variability of droughts through a multi-temporal analysis approach of past droughts. A qualitative investigation was applied for highlighting commonalities between the spatio-temporal development of different panEuropean droughts of the last 50 years by Parry et al. (2012). From a different perspective, Sheffield et al. (2012) proved the significance of the chosen evapotranspiration method in estimation of trend, using the PDSI meteorological index in order to compare the trends using Thornthwaite and Penman-Monteith estimation of evapotranspiration methods. Dai (2012) studied how droughts might change under increasing greenhouse gas (GHG), through analyzing coupled climate model simulations under intermediate future GHG emissions scenarios from the Coupled Model Intercomparison Project phase 3 (CMIP3) and the new phase 5 (CMIP5). Finally, another approach was that of Lehner et al. (2006), which was based on the frequency analysis instead of trend.

1.5 Investigation of future droughts

Nevertheless, the global warming, the increased climate variability, and the increased trend on droughts the last decades, have oriented the study interest of the scientists in future evolution, characteristics and frequency of droughts. The development of robust global gridded re-analysis dataset, e.g. WATCH (WATer and global CHange) Forcing Data or CMIP5 (Coupled Model intercomparison Project Phase 5), the General Circulation Models (GCMs) and the Global Impact Models (GIMs) and the collaboration all of them, is a sign of this direction. More specific, Wanders et al. (2014) investigated the global hydrological droughts in the 21st century under a changing hydrological regime, applying a conventional variable threshold and a transient variable threshold. Likewise, Prudhomme et al. (2013) identified hotspots and uncertainties of global hydrological droughts from a global multimodel ensemble experiment for the last 30 years of the 21st century. Based on the same technique Wanders and Van Lanen, (2013) investigated the future

discharge drought across climate regions around the world modelled with a synthetic hydrological modelling approach.

1.6 Objective

The purpose of this study is, using the outcomes of WATCH project to estimate the SPI and SPEI drought indices for the future period of 2001-2100 and verify how droughts proceed in comparison with the historical period of 1961-1990. It is done for the outcomes of three GCMs in order to be sure that all models are in agreement and give reliable results. Additionally, the outcomes for two future climate scenarios each model are examined.

1.7 The structure of the present work

The remainder of this thesis is organized as follows: first, the background of the WATCH project is summarized and so the data as the study area are introduced. Afterwards, in the background section, a comprehensive description of what SPI and SPEI are, is presented. In the section of methodology, the exactly procedures for the calculation of the indices are shown. All the modifications on the original procedure are mentioned and described, also. Afterwards, the exposition of the results follows in the respective section, while the discussion and the interpretation of them is done in the correspond section.

2 Data and study site

2.1 WATCH Project

The present work is based on the available data of WATCH (Water and Global Change) project. The WATCH project has produced a large number of data sets which should be of considerable use in regional and global studies of climate and water. Some of these datasets are described in the special collection, particularly Weedon et al. (2011) and Haddeland et al. (2011). These data are all hosted by IIASA in Austria on a basic FTP site available to the public[2].

More specific, all the available data sets from WATCH project are represented below[3]:

[2] http://www.eu-watch.org/data_availability
[3] http://www.eu-watch.org/data_availability

- **WATCH Forcing Data 20th Century**: a meteorological forcing dataset (based on ERA-40) for land surface and hydrological models (1901-2001). Five variables are at 6 hourly resolution and five variables are at 3 hourly resolution.
- **WATCH-Forcing-Data-ERA-Interim**: WFDEI was produced post-WATCH using WFD methodology applied to ERA-Interim data. It is a meteorological forcing dataset extending into early 21st C (1979 – 2012). Eight meteorological variables at 3-hourly time steps, and as daily averages.
- **WATCH Driving Data 21st Century**: similar to the WATCH forcing data but for the 21st Century and is constructed from model output not interpolated observational data. Two climate scenarios, B1, A2 and a Control were each run through three global climate models (CNRM, ECHAM5 and IPSL) to produce a total of 9 sets of future driving data at 0.5 degree resolution.
- **WATCH 20th Century Model Output Datasets**: the WATCH forcing data has been run through nine land surface or global hydrological models, to produce a range of output variables.
- **WATCH 21st Century Model Output**: the 21st century WATCH driving data was put through ten land surface and global hydrological models. 20th Century Ensemble Data: ensemble of model output data from 5 models for 4 hydrological variables, stored as daily data in monthly NetCDF files
- **Test Basin data**: 21st C driving data for each test basin (Crete, Glomma, Nitra, Upper-Elbe, Upper Guadiana)

The present thesis is based on the data set of WATCH Driving Data 21st Century. The WATCH Driving data is a twenty-first century meteorological driving dataset for land surface and hydrological models. It consists of daily states of the weather for global 0.5 degree grid points but excludes Antarctica. It was generated as part of the 6th Framework Programme (FP6) of European Research project "WATCH" (WATer and global CHange") which ran from 2007-2011. Daily data is available from 2001 through to 2100. Two climate scenarios, B1, A2 and a Control are each run through three global climate models, CNRM, ECHAM5 and IPSL to produce a total of nine sets of future driving data as they are represented in figure 1. Data is at daily resolution, variables include mean daily temperature in K (T), min. daily temperature in K (Tmin), max. daily temperature in K (Tmax), total precipitation in mm/s (pr), snow precipitation in mm/s (pr_SNOWF), surface specific humidity inkg/kg (huss), surface air pressure in Pa (ps), surface downwelling longwave flux in air in W/m2 (rsds), wind speed at 10m in m/s (wss), net IR rad. at surface (soll)

solldown and mean daily temperature in K (tas). All the variables in the WATCH Driving Data historical period are bias corrected. Only temperature and precipitation are bias corrected in the future runs. The methodology of bias correction is described by Hagemann et al. (2011). Finally, each GCM model gives Bias Corrected, Original Gregorian and Original data[4].

But, although, the data set offers all these variables, one part of them was used. More specifically, the total precipitation and snow precipitation were used for the calculation of SPI drought index. Whereas, total precipitation, snow precipitation, mean, maximum and minimum daily temperature and wind speed were used for the calculation of SPEI drought index. Actually, the total and snow precipitation were used in order to define the rain precipitation as the difference between them.

As it aforementioned, two time periods where were used, one as control period and one as future period. The control period corresponds to the 30 years period between 1961 and 1990, whereas the future period corresponds to the whole 21st century (2001-2100). As concerns the control period, a 30 years period was chosen, although the available data was for the period 1960-2000 (41years). This selection was done because the 30 years period has set in as reference period from the majority of the scientists. So, this period was chosen in order to be the results comparable with the results of other works. Finally, for consistency, leap years were shortened to a 365 day calendar year by censoring the final day of the year.

Concluded, it should be noticed that, all the WATCH data is in NetCDF format (Network Common Data Format), which is an extremely efficient data format for large volumes of data and is popular with modellers as both an input and output format.

[4] http://data-search.nerc.ac.uk/search/full/catalogue/ceh.nerc.ac.uk__NERC_DMS_0.7__1317910387047.xml

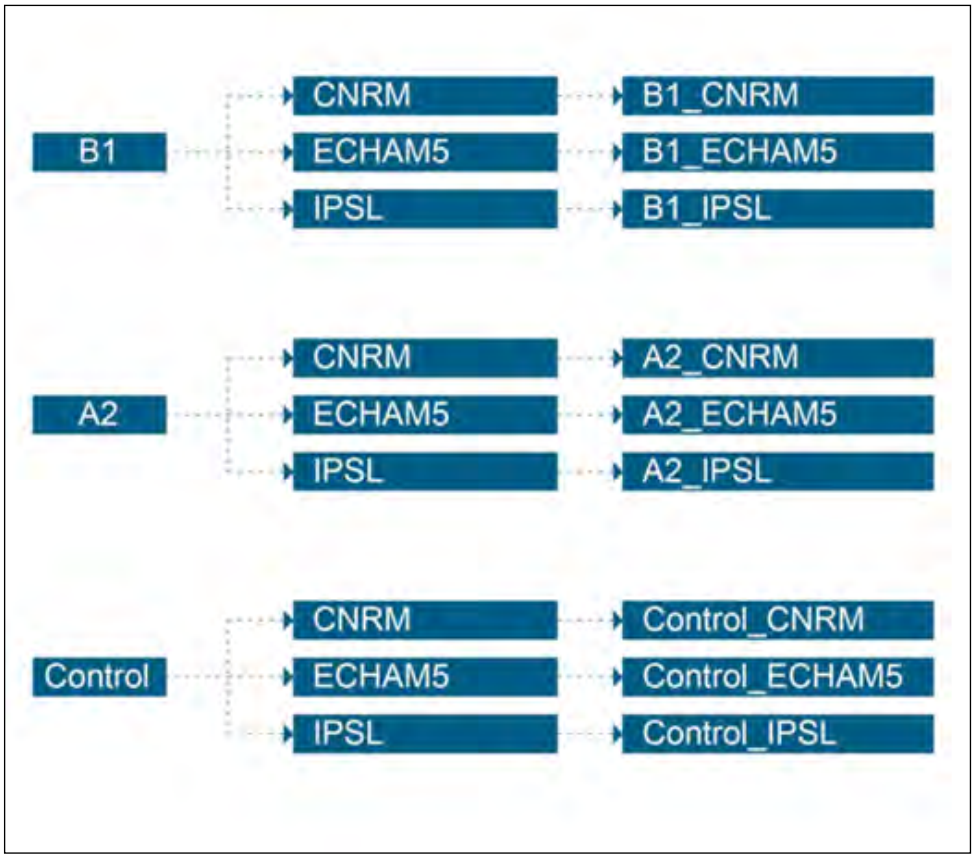

Figure 1: Flow chart which represents the 9 sets of future driving data[5].

2.2 Study area

As concerns the study area, for the purpose of this research, Greece area is defined as the region between 33°43° N latitude and 18°30° E longitude. This area exceeds the border of the country. But, because drought is regional phenomenon, the extension of the research out of the border gives a more enlightening image about what happens in Greece. Also, in case of existing spatial patterns of the drought indices, this extend helps to identify them.

The present investigation of droughts concerns only the land of Greece. Based on that the area which corresponds to sea surface has removed from the analysis. Additionally, due to the fact that drought can occurs in any climate or region on Earth according to the definition Tallaksen and Van Lanen (2004), the relief of Greece and the wider area is not linked with the occurrence of drought.

Finally, figure 2 presents the maps of Greece and its wider area which was taken into consideration. This maps is covered by the of 0.5° grid points, in which the WATCH data is available.

[5] http://www.waterandclimatechange.eu/about/watch-driving-data-21st-century

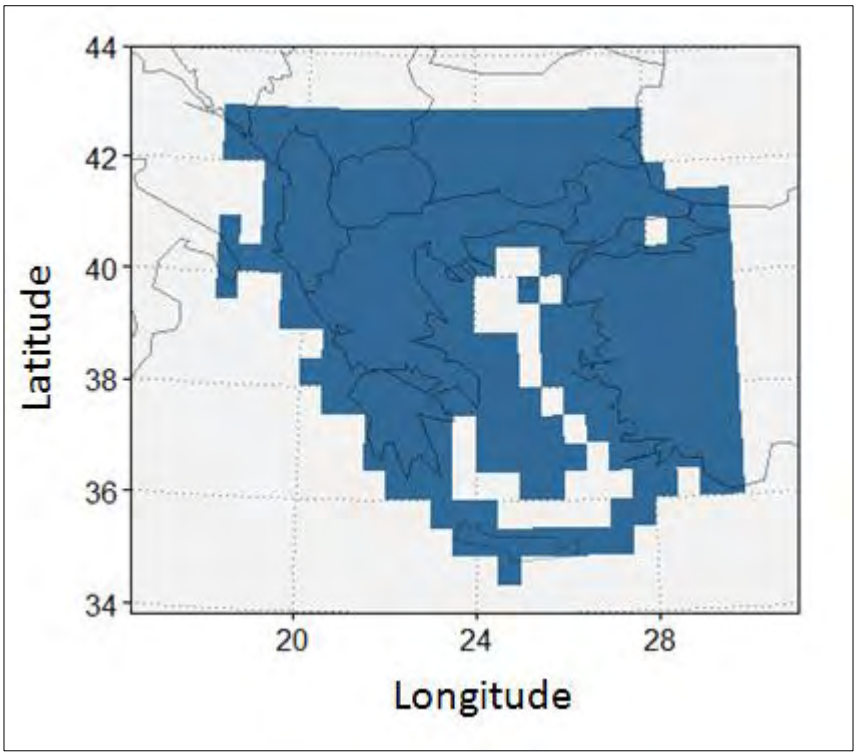

Figure 2: This picture with the selected 0.5 degrees cells which correspond in the land of our case study.

2.3 General Circulation models

2.3.1 General description of GCMs

According to the description of Intergovernmental Panel on Climate Change (IPCC) (IPCC-TGICA, 2007, GCMs or General Circulation Models are numerical models which represent physical processes in the atmosphere ocean, cryosphere and land surface. Nowadays, they are the most advanced tools available for simulating the response of global climate system to increasing greenhouse gas concentrations. While simpler models exist to provide globally - or regionally - averaged estimates of the climate response, only GCMs, possibly in conjunction with nested regional models, have the potential to provide geographically and physically consistent estimates of regional climate change which are required in impact analysis.

GCMs depict the climate using a three dimensional grid over the globe (Figure 3), typically having a horizontal resolution of between 250 and 600 km, 10 to 20 vertical layers in the atmosphere and sometimes as many as 30 layers in oceans. Their resolution is thus quite coarse relative to the scale of exposure units in most impact assessments. Moreover, many physical processes, such as those related to

clouds, also occur at smaller scales and cannot be properly modeled. Instead , their known properties must be averaged over the larger scale in a technique known as parameterization. This is one source of uncertainty in GCM-based simulations of the future climate. Others relate to the simulation of water vapour and warming, clouds and radiation, ocean circulation and ice and snow albedo. For this reason, GCMs may simulate quite different responses to the same forcing, simply because of the way certain processes and feedbacks are modelled (IPCC-TGICA, 2007).

However, while these differences in response are usually consistent with the climate sensitivity, they are unlikely to approach the uncertainty range of regional projections. Even the selection of all the available GCM experiments would not guarantee a representative range, due to other uncertainties that GCMs don't fully address, especially the range in estimates of future atmospheric composition (IPCC-TGICA, 2007).

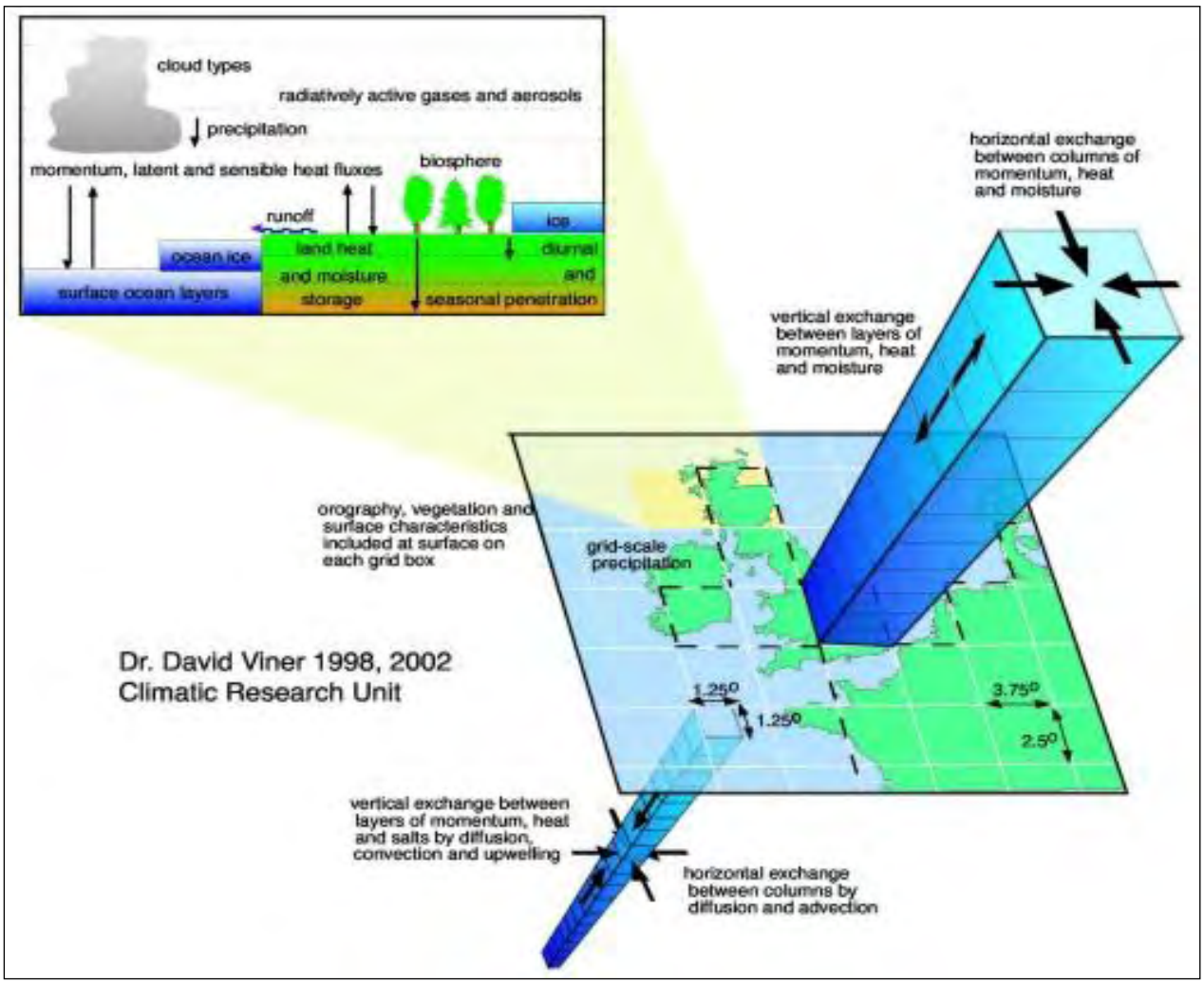

Figure 3: Conceptual structure of a coupled atmosphere-ocean general circulation model. Source: Viner and Hulme (1997).

2.3.2 ECHAM5, CNCRM and IPSL GCMs

As it aforementioned above, the "WATCH diving data 21st Century" is produced by the outcomes of three GCMs. As concerns that three GCMs, they are presented in the below. The ECHAM5/Max Planck Institute Ocean Model (MPI-OM) is the first one, the Centre National de Recherches Météorologiques Coupled GCM, version3 (CNRM-CM3) is the second and the atmospheric component of the L'Institut Pierre-Simon Laplace Coupled Model, version 4 (IPSL CM4) coupled model is the last one.

Hagemann et al. (2011), on his work regarding the impacts of statistical bias correction of climate model outputs, described briefly but substantive the three used GCMs. This description follows below:

ECHAM5

The coupled atmosphere–ocean GCM ECHAM5–Max Planck Institute Ocean Model (MPI-OM) (denoted simply ECHAM5 henceforth; Roeckner et al. 2003;Jungclaus et al. 2006) of the Max Planck Institute for Meteorology (MPI-M) has been used to conduct an ensemble of climate simulations. The GCM takes into account concentrations of CO_2, CH_4, N_2O, chlorofluorocarbons (CFCs), O_3 (tropospheric and stratospheric), and sulfate aerosols, thereby considering the direct and first indirect aerosol effect.

CNRM

The Centre National de Recherches Météorologiques Coupled GCM, version 3 (CNRM-CM3;henceforth simply CNRM) comprises the submodels Action de Recherche Petite Echelle Grande Echelle (ARPEGE)-Climat version 3 for the atmosphere (Dequé et al. 1994;Déqué and Piedelievre 1995; Royer et al. 2002), Océan Parallelisé (OPA) 8.1 for the ocean (Madec et al. 1998),and GELATO 2 for sea ice (Salas-Mélia 2002). The distributions of marine, desert, urban aerosols, and sulfate aerosols were specified, whereas for aerosols only the direct effect of anthropogenic sulfate aerosols was taken into account.

IPSL

The L'Institut Pierre-Simon Laplace Coupled Model, version 4 (IPSL CM4; hereafter simply IPSL) includes the submodels LMDZ-4 for the atmosphere (Hourdin et al. 2006), ORCA for the ocean (based on the OPA model; Madec et al. 1998), and LIM for sea ice (Fichefet and Morales Maqueda 1997; Goosse and Fichefet 1999). With regard to prescribed aerosols, the direct effect of sulfate aerosols was taken into account, as well as the first indirect effect.

2.4 Scenario

2.4.1 Definition of scenario

A scenario is a coherent, internally consistent and plausible description of a possible future state of the world (IPCC, 1994). It is not a forecast; rather, each scenario is one alternative image of how the future can unfold. A projection may serve as the raw material for a scenario, but scenarios often require additional information (e.g., about baseline conditions). A set of scenarios is often adopted to reflect, as well as possible, the range of uncertainty in projections (IPCC-TGICA,2007).

2.4.2 The SRES emissions scenarios

As the IPCC-TGICA, 2007 outlined, the IPCC published a set of emissions scenarios in 2000 for use in climate change studies (Special Report on Emissions Scenarios – SRES). The SRES scenarios were constructed to explore future developments in the global environment with special reference to the production of greenhouse gases and aerosol precursor emissions. The report adopted the following terminology:

- Storyline: a narrative description of a scenario (or a family of scenarios), highlighting the main scenario characteristics and dynamics, and the relationships between key driving forces.
- Scenario: projections of a potential future, based on a clear logic and a quantified storyline.
- Scenario family: one or more scenarios that have the same demographic, politico-societal, economic and technological storyline.

The SRES team defined four narrative storylines (Figure 4), labelled A1, A2, B1 and B2, describing the relationships between the forces driving greenhouse gas and aerosol emissions and their evolution during the 21st century for large world regions and globally. Each storyline represents different demographic, social, economic, technological, and environmental developments that diverge in increasingly irreversible ways (IPCC-TGICA,2007)

.

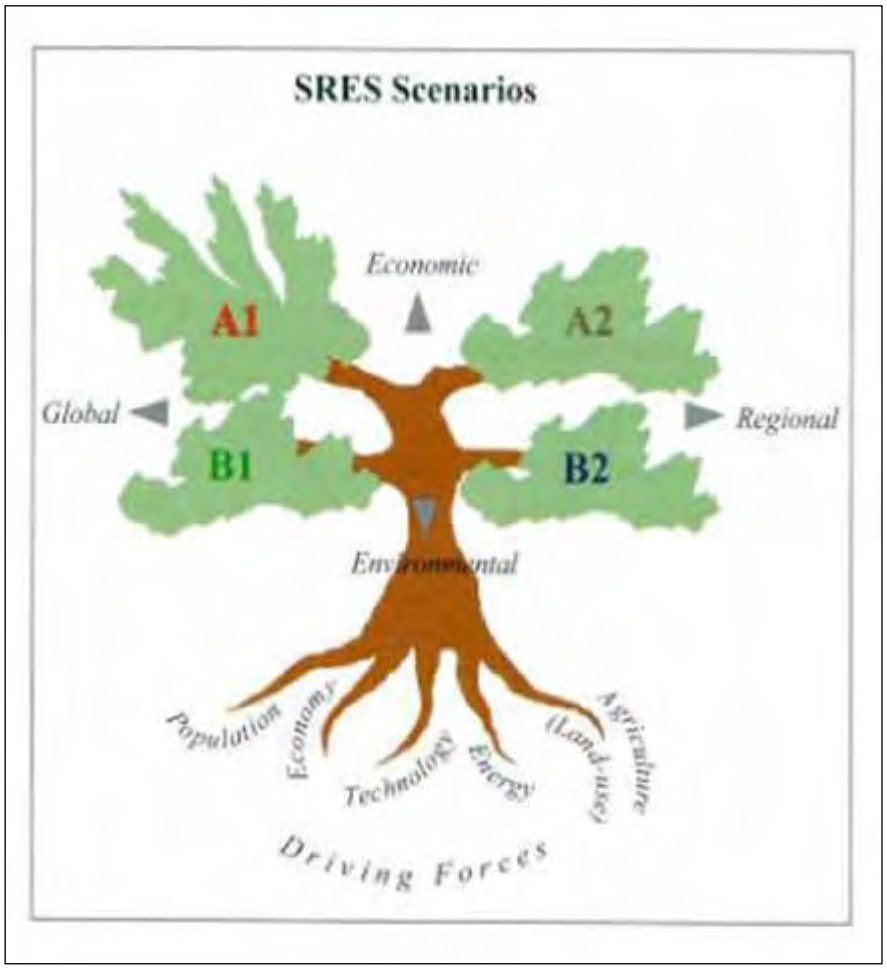

Figure 4: Schematic illustration of the four SRES storylines (after Nakićenović et al., 2000).

In simple terms, the four storylines combine two sets of divergent tendencies: one set varying between strong economic values and strong environmental values, the other set between increasing globalization and increasing regionalization . The storylines are summarized as follows (Nakićenović et al., 2000):

- A1 storyline and scenario family: a future world of very rapid economic growth, global population that peaks in mid-century and declines thereafter, and rapid introduction of new and more efficient technologies.

- A2 storyline and scenario family: a very heterogeneous world with continuously increasing global population and regionally oriented economic growth that is more fragmented and slower than in other storylines.
- B1 storyline and scenario family: a convergent world with the same global population as in the A1 storyline but with rapid changes in economic structures toward a service and information economy, with reductions in material intensity, and the introduction of clean and resource-efficient technologies.
- B2 storyline and scenario family: a world in which the emphasis is on local solutions to economic, social, and environmental sustainability, with continuously increasing population (lower than A2) and intermediate economic development.

2.5 Baseline period

The baseline period is usually selected according to the following criteria (IPCC, 1994):

- representative of the present-day or recent average climate in the study region.
- of a sufficient duration to encompass a range of climatic variations, including a number of significant weather anomalies (e.g. severe droughts or cool seasons).
- covering a period for which data on all major climatological variables are abundant, adequately distributed over space and readily available.
- including data of sufficiently high quality for use in evaluating impacts.
- consistent or readily comparable with baseline climatologies used in other impact assessments.

A popular climatological baseline period is a 30-year "normal" period as defined by the World Meteorological Organisation (WMO) (IPCC, 1994). The current WMO normal period is 1961-1990. As well as providing a standard reference to ensure comparability between impact studies, other advantages of using this baseline period include:

- The period ends in 1990, which is the common reference year used for climatic and non-climatic projections by the IPCC in the First and Second Assessment Reports (and retained for the Third Assessment Report).
- It represents the recent climate, to which many present-day human or natural systems are likely to have become reasonably well adapted (though there are

exceptions, such as vegetation zones or groundwater levels, that can have a response lag of many decades or more relative to the ambient climate).

- In most countries, the observed climatological data are most readily available for this period, especially in computer-coded form at a daily time resolution.

3 Background

3.1 SPI drought index

3.1.1 Introduction

As it outlined in WMO SPI User Guide (2012)), the Standardized Precipitation Index (SPI) is a tool which was developed primarily for defining and monitoring drought. It allows an analyst to determine the rarity of a drought at a given time scale (temporal resolution) of interest for any rainfall station with historic data. It can also be used to determine periods of anomalously wet events. The SPI is not a drought prediction tool.

A real strength of the SPI is its ability to be calculated for many timescales, which makes it possible to deal with many of the drought types (agricultural, hydrological, meteorological etc). The ability to compute the SPI on multiple timescales allows for temporal flexibility in the evaluation of precipitation conditions in relation to water supply (WMO SPI User Guide (2012)).

The SPI was designed to quantify the precipitation deficit for multiple timescales, or moving averaging windows. These timescales reflect the impacts of drought on different water resources needed by various decision-makers. Meteorological and soil moisture conditions (agriculture) respond to precipitation anomalies on relatively short timescales, for example 1-6 months, whereas streamflow, reservoirs, and groundwater respond to longer-term precipitation anomalies of the order of 6 months up to 24 months or longer. So, for example, one may want to look at a 1- or 2-month SPI for meteorological drought, anywhere from 1-month to 6-month SPI for agricultural drought, and something like 6-month up to 24-month SPI or more for hydrological drought analyses and applications (WMO SPI User Guide (2012)).

3.1.2 Creation of aggregated data for different time scales

The precipitation values can be aggregated at different temporal scales. The precipitation $p_{i,j}^{k}$ in a given month j and year i, depends on the chosen time scale k.

For example, the accumulated precipitation for one month in a particular year i with a 12-month time scale is calculated using

$$p_{i,j}^{k} = \sum_{l=13-k+j}^{12} p_{i-1,l} + \sum_{l=1}^{j} p_{i,l} \qquad \text{for } j < k,$$

and

$$p_{i,j}^{k} = \sum_{l=j-k+1}^{j} p_{i,l} \qquad \text{for } j \geq k$$

where $p_{i,l}$ is the precipitation in the first month of the year i, in millimeters.

3.1.3 Computation of SPI

In the following subsection, all the steps for the computation of the SPI follow[6]. Originally, the α and β parameters are estimated through the maximum likelihood estimation using the approximation of Thom, 1958:

$$\hat{\alpha} = \frac{1}{4A}\left(1 + \sqrt{\frac{4A}{3}}\right) \; and \; \hat{\beta} = \frac{\bar{x}}{\hat{\alpha}}$$

where for n observations

$$A = \ln(\bar{x}) - \frac{\sum \ln(x)}{n}$$

The estimated parameters are then used for calculating cumulative probability distribution for a specific precipitation event, which has been observed on a defined time scale (e. g. month):

$$G(x) = \int_0^x g(x)dx = \frac{1}{\hat{\beta}^{\hat{\alpha}}\Gamma(\hat{\alpha})}\int_0^X x^{\hat{\alpha}} e^{-x/\hat{\beta}}\, dx$$

substituting t for $-x/\hat{\beta}$ yields the incomplete gamma function:

[6] http://www.dmcsee.org/uploads/file/70_drought_indices_a_ceglar.pdf

$$G(x) = \frac{1}{\Gamma(\hat{\alpha})} \int_0^x t^{\hat{\alpha}-1} e^{-t}\, dt$$

The gamma distribution is undefined for x = 0 and q = P(x = 0) > 0, where P(x = 0) is the probability of zero (null) precipitation. Thus, the cumulative probability distribution function becomes:

$$H(x) = q + (1 - q) * G(x)$$

where q is the probability of no rainfall on specified time scale.

Cumulative probability distribution H(x) is then transformed into standardized normal distribution Z with the average equal to 0 and standard deviation 1. SPI is number of standard deviations from 0 (Figure 5). The negative deviations denote drought, while the positive deviations denote wet.

Transformation from given probability distribution into different probability distribution is applying, according to Panofsky in Birer (1958). More specific, the probability that the value of variable is less than some value in defined probability distribution must be identical to probability of the transformed variable being less than transformed value in second probability distribution.

Transformation of cumulative probability distribution H(x) into standardized normal distribution (Abramowitz and Stegun, 1965):

$$z = SPI = -\left(t - \frac{c_0 + c_1 t + c_2 t^2}{1 + d_1 t + d_2 t^2 + d_3 t^3}\right) \quad \text{for} \quad 0.5 < H(x) < 1.0 \;\; t = \sqrt{\ln\left(\frac{1}{(H(x))^2}\right)}$$

$$z = SPI = +\left(t - \frac{c_0 + c_1 t + c_2 t^2}{1 + d_1 t + d_2 t^2 + d_3 t^3}\right) \quad \text{for} \quad 0 < H(x) < 0.5 \quad t = \sqrt{\ln\left(\frac{1}{(H(x))^2}\right)}$$

. The constants are: $c_o = 2.515517$, $c_1 = 0.802853$, $c_2 = 0.010328$, $d_1 = 1.432788$, $d_2 = 0.189269$, $d_3 = 0.001308$.

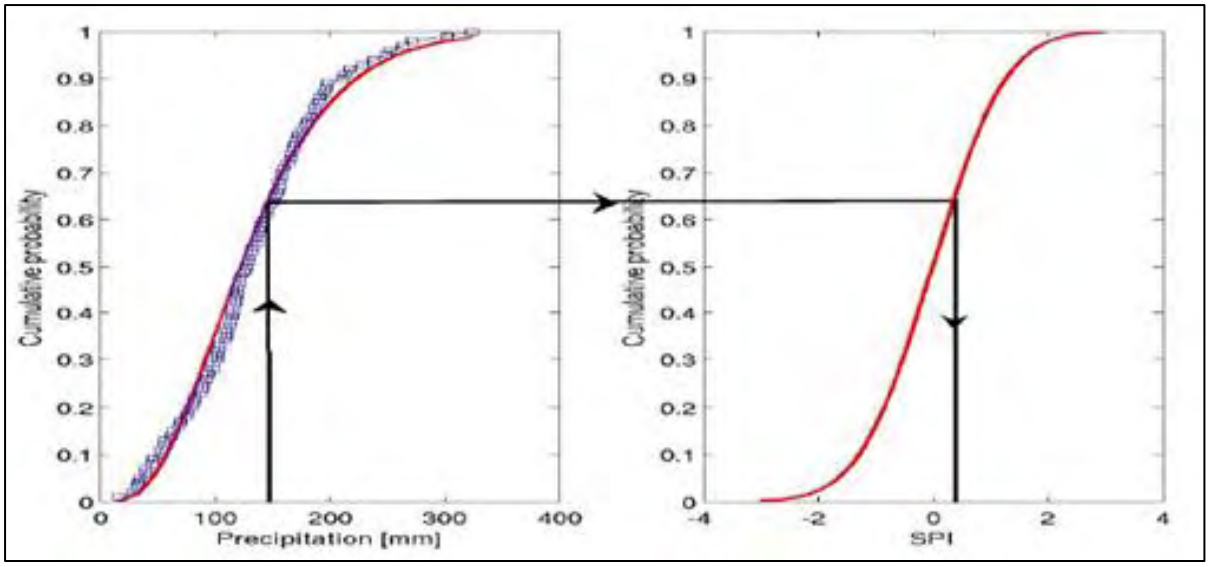

Figure 5: Transformation from cumulative probability distribution into standardized normal distribution.

Finally, McKee and others (1993) used the classification system which is shown on the Table 2 in order to define drought intensities resulting from the SPI values. They also defined the criteria for a drought event for any of the timescales. A drought event occurs any time the SPI is continuously negative and reaches an intensity of -1.0 or less. The event ends when the SPI becomes positive. Each drought event, therefore, has a duration defined by its beginning and end, and an intensity for each month that the event continues. The positive sum of the SPI for all the months within a drought event can be termed the drought's "magnitude".

Table 2: SPI values classification.

SPI	Classification	Probability (%)
2.0>	Extremely wet	2.3
1.5 to 1.99	Very wet	4.4
1.0 to 1.49	Moderately wet	9.2
0 to 0.99	Mildly wet	34.1
0 to -0.99	Mildly drought	34.1
-1.0 to -1.49	Moderately drought	9.2
-1.5 to -1.99	Severely drought	4.4
-2.0 <	Extremely drought	2.3

3.2 SPEI drought index

3.2.1 Introduction

In fact, the SPEI is analogous and is based on the calculation procedure of SPI. Instead of solely using monthly precipitation as its input data (as the SPI does), the SPEI uses monthly difference between precipitation and potential evapotranspiration (PET), which stands for a simple climatic water balance (Vicente-Serrano et al., 2010).

$$d_i = P_i - PET_i$$

So, the main differences in the computation of SPI and SPEI are concentrated in calculation of the potential evapotranspiration and the probability distribution function for the fitting of the accumulated differences between precipitation and potential evapotranspiration.

3.2.2 Creation of aggregated data for different time scales

In the original version of the SPEI, the Thornthwaite equations (Thornthwaite, 1948) are used. So, with a value for *PET*, the difference between the precipitation (*P*) and *PET* for the month *i* is calculated:

$$d_i = P_i - PET_i,$$

which provides a simple measure of the water surplus or deficit for the analyzed month.

Below the Thornthwaite method (Thornthwaite,1948) is presented, as it was outlined by Vicente-Serrano et al., (2010). This method was chosen because it was the simplest approach to calculate PET, which has the advantage of only requiring data on monthly-mean temperature. Following this method, the monthly PET (mm) is obtained by

$$PET = 16K\left(\frac{10T}{I}\right)^m,$$

where T is the monthly-mean temperature (8°C); I is a heat index, which is calculated as the sum of 12 monthly index values i, the latter being derived from mean-monthly temperature using the formula

$$i = \left(\frac{T}{5}\right)^{1.514}$$

m is a coefficient depending on I: $\mathrm{m} = 6.75 * 10^{-7}\mathrm{I}^3 - 7.71 * 10^{-5}\mathrm{I}^2 + 1.79 * 10^{-2}\mathrm{I} + 0.492$; and K is a correction coefficient computed as a function of the latitude and month,

$$K = \left(\frac{N}{12}\right)\left(\frac{NDM}{30}\right).$$

Here NDM is the number of days of the month and N is the maximum number of sun hours, which is calculated using

$$N = \left(\frac{24}{\pi}\right)\overline{\omega_s}$$

where $\overline{\omega_s}$ is the hourly angle of sun rising, which is calculated using

$$\overline{\omega_s} = \arccos(-\tan\varphi \tan\delta)$$

where φ is the latitude in radians and δ is the solar declination in radians, calculated using

$$\delta = 0{,}4093\mathrm{sen}\left(\frac{2\pi \mathrm{J}}{365} - 1.405\right)$$

where J is the average Julian day of the month.

Then, the calculated $\mathrm{d_i}$ values can be aggregated at different temporal scales, following the same procedure as that for the SPI. Te difference $\mathrm{d_{i,j}^k}$ in a given month j and year i, depends on the chosen time scale k. For example, the accumulated difference for one month in a particular year i with a 12-month time scale is calculated using

$$\mathrm{d_{i,j}^k} = \sum_{\mathrm{l=13-k+j}}^{12} \mathrm{d_{i-1,l}} + \sum_{\mathrm{l=1}}^{\mathrm{j}} \mathrm{d_{i,l}} \qquad \text{for } \mathrm{j} < k,$$

and

$$\mathrm{d_{i,j}^k} = \sum_{\mathrm{l=j-k+1}}^{\mathrm{j}} \mathrm{d_{i,l}} \qquad \text{for } \mathrm{J} \geq \mathrm{k}$$

where $\mathrm{d_{i,l}}$ is the $\mathrm{P} - \mathrm{PET}$ in the first month of the year i, in millimeters.

3.2.3 Computation of SPEI

Selection of the most suitable statistical distribution to model the differences d series was difficult, given the similarity among the four distributions (Pearson III, Lognormal, Log-logistic and General Extreme Value). The selection was based on the behaviour at the most extreme values. Log-logistic distribution showed a gradual decrease in the curve for low values, and coherent probabilities were obtained for very low values of d, corresponding to 1 occurrence in 200 to 500 years. Additionally, no values were found below the origin parameter of the distribution.

The probability density function of a three parameter Log-logistic distributed variable is expressed as:

$$f(x) = \frac{\beta}{\alpha}\left(\frac{x-\gamma}{\alpha}\right)^{p-1}\left(1+\left(\frac{x-\gamma}{\alpha}\right)^{p}\right)$$

where α, β and γ are scale, shape and origin parameters, respectively, for d values in the range (γ > d < ∞).

Parameters of the Log-logistic distribution can be obtained following different procedures. Among them, the L-moment procedure is the most robust and easy approach (Ahmad et al., 1988). When L-moments are calculated, the parameters of the Pearson III distribution can be obtained following Singh et al. (1993):

$$\beta = \frac{2W_1 - W_0}{6W_1 - W_0 - 6W_2}$$

$$a = \frac{(W_0 - 2W_1)\beta}{\Gamma\left(1+\frac{1}{\beta}\right)\Gamma\left(1+\frac{1}{\beta}\right)}$$

$$\gamma = W_0 - \alpha\Gamma\left(1+\frac{1}{\beta}\right)\Gamma\left(1-\frac{1}{\beta}\right)$$

where Γ(β) is the gamma function of β.

In Vicente-Serrano et al. (2010), when the log-logistic α, β and γ distribution parameters were calculated, the probability weighted moments (PWMs) method was used, based on the plotting-position approach (Hosking, 1990), where the PWMs of order s are calculated as:

$$w_s = \frac{1}{N}\sum_{i=1}^{N}(1-F_i)^S D_i$$

where N is the number of data, F_i is a frequency estimator following the approach of Hosking (1990) and D_i is the difference between Precipitation and Potential Evapotranspiration for the month i.

The probability distribution function of *D* according to the Log-logistic distribution is then given by:

$$F(x) = \left[1 + \left(\frac{a}{x-\gamma}\right)^{\beta}\right]^{-1}$$

With F(*x*) the SPEI can easily be obtained as the standardized values of F(*x*). For example, following the classical approximation of Abramowitz and Stegun, 1965:

$$SPEI = W - \frac{C_0 + C_1 W + C_2 W^2}{1 + d_1 W + d_2 W^2 + d_3 W^3}$$

where

$$W = -2\ln(P),$$

for $P \leq 0.5$, *P* being the probability of exceeding a determined *D* value, $P = 1 - F(x)$. If $P > 0.5$, *P* is replaced by $1-P$ and the sign of the resultant SPEI is reversed. The constants are: $C0 = 2.515517$, $C1 = 0.802853$, $C2 = 0.010328$, $d1 = 1.432788$, $d2 = 0.189269$, $d3 = 0.001308$. The average value of the SPEI is 0, and the standard deviation is 1. The SPEI is a standardized variable, and it can therefore be compared with other SPEI values over time and space. An SPEI of 0 indicates a value corresponding to 50% of the cumulative probability of *d*, according to a Log-logistic distribution[7].

4 Methodology

4.1 SPI index

4.1.1 Aggregated data at daily temporal resolution

In this study, as Stagge et al. (2014) proposed, was calculated at daily temporal resolution in contrast with the original definition which uses monthly temporal resolution. The usage of daily time step lets the drought indices retains the higher resolution of the original data, giving more details and accuracy within months e.g.

[7] http://sac.csic.es/spei/home.html

we are able to know the exact date of the start-end day of a drought event during the months. In addition, this kind of data retains monthly averaged. In the present work, the accumulated periods of 1, 3, 6 and 12 months were examined which correspond to 30, 91, 183 and 365 days, respectively. But in order to be the results more understandable and comparable with previous studies, we call the SPI of 30 days accumulation period SPI-1, the SPI of 91 days accumulation period SPI-3 etc. Furthermore, using a daily resolution requires fitting 365 parametric probability distributions, rather than 12 distributions, which, also, gives more detail and smoother transitions (Stagge et al., 2014).

So, the precipitation values can be aggregated at different temporal scales, again. Now, the precipitation $p_{i,j}^{k}$ represents the given day j and year i, instead for month and year, respectively. For example, the accumulated precipitation for one day in a particular year i with a 12-month (365-days) time scale is calculated using

$$p_{i,j}^{k} = \sum_{l=366-k+j}^{365} p_{i-1,l} + \sum_{l=1}^{j} p_{i,l} \qquad \text{for } j < k,$$

and

$$p_{i,j}^{k} = \sum_{l=j-k+1}^{j} p_{i,l} \qquad \text{for } J \geq k$$

where $p_{i,l}$ is the precipitation in the first day of the year i, in millimeters.

This procedure is applied so for the control period as for the future period (21st Century).

4.1.2 Computation of SPI for the control period

The aggregated data at daily temporal resolution is ready. Afterwards, the α and β parameters are estimated through the maximum likelihood estimation using the approximation of Thom, 1958. The same formulas, as they were presented in subsection 3.1.3, were used and they are presented again below:

$$\hat{\alpha} = \frac{1}{4A}\left(1 + \sqrt{\frac{4A}{3}}\right) \; and \; \hat{\beta} = \frac{\bar{x}}{\hat{\alpha}}$$

where for n observations

$$A = \ln(\bar{x}) - \frac{\sum \ln(x)}{n}$$

and

x : the values of the sample.

Using a daily resolution requires fitting 365 parametric probability distribution, one for the first day of the year, one for the second etc. So, the parameters for each day of the year were estimated. The fact that control period consists from 30 years means the for the estimation of the parameters of each day, 30 values are available. Finally, 365 pair of parameters per cell are arisen. This procedure is repeated for the 270 cells of our study area.

The next step is the calculation of the cumulative probability distributions using the estimated parameters. The gamma distribution is selected according to the original definition of SPI (McKee et al., 1993).

$$G(x) = \int_0^x g(x)dx = \frac{1}{\hat{\beta}^{\hat{\alpha}}\Gamma(\hat{\alpha})}\int_0^X x^{\hat{\alpha}} e^{-x/\hat{\beta}}\,dx$$

substituting t for $-x/\hat{\beta}$ yields the incomplete gamma function is:

$$G(x) = \frac{1}{\Gamma(\hat{\alpha})}\int_0^X t^{\hat{\alpha}-1} e^{-t}\,dt$$

The gamma distribution is undefined for x = 0 and q = P(x = 0) > 0, where P(x = 0) is the probability of zero (null) precipitation. Thus, the cumulative probability distribution function becomes:

$$H(x) = q + (1 - q) * G(x)$$

where q is the probability of no rainfall on specified time scale. So, 365 gamma cumulative probability distributions for each of the 270 cells are defined

Afterwards, each cumulative probability distribution H(x) is transformed into standardized normal distribution Z with the average equal to 0 and standard deviation 1. SPI is number of standard deviations left (drought) or right (wet) from 0.

Transformation from given probability distribution into different probability distribution is applying, according to Panofsky in Birer (1958). More specific, the probability that the value of variable is less than some value in defined probability distribution must be identical to probability of the transformed variable being less than transformed value in second probability distribution.

Transformation of cumulative probability distribution H(x) into standardized normal distribution (Abramowitz and Stegun, 1965):

$$z = SPI = -\left(t - \frac{c_0 + c_1 t + c_2 t^2}{1 + d_1 t + d_2 t^2 + d_3 t^3}\right) \quad \text{for} \quad 0.5 < H(x) < 1.0 \quad t = \sqrt{\ln\left(\frac{1}{(H(x))^2}\right)}$$

$$z = SPI = +\left(t - \frac{c_0 + c_1 t + c_2 t^2}{1 + d_1 t + d_2 t^2 + d_3 t^3}\right) \quad \text{for} \quad 0 < H(x) < 0.5 \quad t = \sqrt{\ln\left(\frac{1}{(H(x))^2}\right)}$$

By this way, the SPI for the control period was calculated. This procedure is followed for the outcomes of the three GCMs models.

4.1.3 Computation of SPI for the 21st Century

Next step is the estimation of the SPI index for the 21st Century. For this purpose, another procedure is followed. Specifically, the step of parameters estimation is skipped. Using the distribution parameters of the control period, the cumulative probability of the future values is defined based on the gamma distribution of the control period. So, using the previous parameters and the future data the next formula is applied :

$$G(x) = \frac{1}{\Gamma(\hat{\alpha})} \int_0^x t^{\hat{\alpha}-1} e^{-t}\, dt$$

The gamma distribution is undefined for x = 0 and q = P(x = 0) > 0, where P(x = 0) is the probability of zero (null) precipitation. Thus, the cumulative probability distribution function becomes:

$$H(x) = q + (1 - q) * G(x)$$

Afterwards, each cumulative probability $\mathrm{H(x)}$ is corresponded to the value of the respective normal distribution of the control period. It is done with the same formula as it described in the subsection 3.1.3 :

$$z = SPI = -\left(t - \frac{c_0 + c_1 t + c_2 t^2}{1 + d_1 t + d_2 t^2 + d_3 t^3}\right) \quad \text{for} \quad 0.5 < H(x) < 1.0 \quad t = \sqrt{\ln\left(\frac{1}{(H(x))^2}\right)}$$

$$z = SPI = +\left(t - \frac{c_0 + c_1 t + c_2 t^2}{1 + d_1 t + d_2 t^2 + d_3 t^3}\right) \quad \text{for} \quad 0 < H(x) < 0.5 \quad t = \sqrt{\ln\left(\frac{1}{(H(x))^2}\right)}$$

. The constants are: $c_o = 2.515517$, $c_1 = 0.802853$, $c_2 = 0.010328$, $d_1 = 1.432788$, $d_2 = 0.189269$, $d_3 = 0.001308$.

The same procedure is repeated for each future dataset so for the B1 scenario, as for the A2 scenario.

That technique gives the advantage of comparing the future droughts conditions over a reference period. In this study, the reference period is the control period. Additionally, following this methodology to approach the future droughts, the arisen indices values stop follow normal distribution. It would be happened only in the ideal case of nothing changing in the cumulative distribution of the future period, assuming a totally steady climate. But, naturally, it is not valid in the case of climate, as climate change has proved.

Finally, the main purpose of this technique, is to feature how the distribution of the droughts will change in the future, assuming as future drought conditions, the drought conditions of the reference period. Of course, if we simplify this family of indices, as the negative deviation from the mean. Then, the distribution of the droughts will be totally different in case of considering the mean of the future period. Actually, they will be normal distributed. So, for example in a drier future climate with lower mean of precipitation, the same value of precipitation will correspond lower deviation than the deviation from a previous period with higher mean. That is why the comparison between a future and a reference period is clearly defined in this work.

4.1.4 Index range limitation

At this point it should be mentioned that SPI values are limited to the range [-3,3] to ensure reasonableness. As it is explained by Stagge et al. (2014), this issue has not been addressed explicitly in previous studies; however, the process of calculating

unbounded SPI values based on the relatively limited historical record requires significant extrapolation and the associated uncertainty.

The point is that we are using 30 years to calculate an SPI of -3, which equates to an event that happens once in 740 years. So, we are already outside our original range. Events outside this range are not removed from the time series, but are designated <-3 or >3 to show that the event is extreme but cannot be accurately quantified. Placing reasonable limits on SPI or providing uncertainty bounds is recommended for all future studies using these indices (Stagge et al., 2014).

4.2 SPEI index

4.2.1 Aggregated data at daily temporal resolution

Exactly the same methodology with SPI is applied to the differences $d = P - PET$ for the calculation of the SPEI. For example, the accumulated precipitation for one day in a particular year i with a 12-month (365-days) time scale is calculated using

$$\mathrm{d}_{\mathrm{i,j}}^{\mathrm{k}} = \sum_{\mathrm{l=366-k+j}}^{365} \mathrm{d}_{\mathrm{i-1,l}} + \sum_{\mathrm{l=1}}^{\mathrm{j}} \mathrm{d}_{\mathrm{i,l}} \qquad \text{for } \mathrm{j} < k,$$

and

$$\mathrm{d}_{\mathrm{i,j}}^{\mathrm{k}} = \sum_{\mathrm{l=j-k+1}}^{\mathrm{j}} \mathrm{d}_{\mathrm{i,l}} \qquad \text{for } \mathrm{J} \geq \mathrm{k}$$

where $\mathrm{d}_{\mathrm{i,l}}$ is the$P - PET$ difference in the first day of the year i, in millimeters.

For the estimation of potential evapotranspiration, the Penman-Montieth with Hargreaves radiation term method (Allen et al., 1998) was chosen instead of Thornthwaite method (Thornthwaite, 1948). This method is referred to here as P-M (Hargreaves).

Hargreaves equation uses the daily difference between Tmax and Tmin as a proxy to estimate net radiation (Hargreaves & Samani, 1985), and simplifies the mass transfer term with a constant. The P-M (Hargreaves) equation uses an identical radiation estimate, but evaluates mass transfer using wind speed from the "WATCH Driving Data 21st Century". The selection of the method done according to Stagge et

al. (2014) regarding the index sensitivity to PET calculation methods. The author conclude saying that "if data permits, the Hargreaves and the P-M (Hargreaves) equations strike a useful balance between consistency and minimal data requirements, requiring only the addition of minimum/maximum temperature and wind speed, in the case of the P-M (Hargreaves)."

Below the presentation of P-M (Hargreaves) follows, as Stage et al. (2014) described. The general formula for the calculation of PET is:

$$\mathrm{PET} = \frac{0.408\Delta(\mathrm{R_n} - \mathrm{G}) + \gamma \frac{900}{\mathrm{T}+273}\mathrm{u_2}(\mathrm{e_s} - \mathrm{e_a})}{\Delta + \gamma(1 + 0.34\mathrm{u_2})}$$

where

PET : potential evapotranspiration [mm day^{-1}],
R_n : net radiation at the crop surface [MJ m^{-2} day^{-1}],
G : soil heat flux density [MJ m^{-2} day^{-1}],
T : mean daily air temperature at 2 m height [°C],
u_2 : wind speed at 2 m height [m s^{-1}],
e_s : saturation vapour pressure [kPa],
e_a : actual vapour pressure [kPa],
e_s- e_a : saturation vapour pressure deficit [kPa],
Δ : slope vapour pressure curve [kPa °C^{-1}],
γ : psychrometric constant [kPa °C^{-1}].

The equation uses standard climatological records of solar radiation (sunshine), air temperature, humidity and wind speed. To ensure the integrity of computations, the weather measurements should be made at 2 m (or converted to that height) above an extensive surface of green grass, shading the ground and not short of water.

Net radiation, R_n, is then calculated as the difference between incoming net shortwave (R_{ns}) and net outgoing longwave (R_{nl}) radiation.

$$R_n = R_{ns} - R_{nl}$$

Net incoming shortwave ($\mathrm{R_{ns}}$) radiation is calculated as :

$$R_{ns} = (1 - a)R_s$$

where

R_{ns} : net solar or shortwave radiation [MJ m^{-2} day^{-1}],

α : albedo or canopy reflection coefficient, which is 0.23 for the hypothetical grass reference crop [dimensionless],

R_s : the incoming solar radiation [MJ m^{-2} day^{-1}]

where the incoming solar radiation (R_s) is based on the Hargreaves and Samani (1985) approximation

$$R_s = k_{R_s}\sqrt{(T_{max} - T_{min})R_a}$$

In this equation, Tmax and Tmin represent maximum and minimum daily temperature (oC), R represents extraterrestrial radiation, and $k_{R_s}$is an adjustment coefficient. For the purpose of this study, k_{R_s} is assumed to be 0.16 for the entire syudy are, though a value of 0.19 may be more applicable for "coastal" locations. Atmospheric radiation, R_a, is calculated from latitude and Julian day by

$$\varphi_r = \frac{\pi}{180}\varphi_d$$

$$d_r = 1 + 0.033\cos\left(\frac{2\pi}{365}J\right)$$

$$\delta = 0.409\sin\left(\frac{2\pi}{365}J - 1.39\right)$$

$$\omega_s = \cos^{-1}(-\tan[\varphi_r]\tan[\delta])$$

$$R_a = \frac{24 \times 60}{\pi}G_{sc}d_r[\omega_s\sin(\varphi_r)\sin(\delta) + \cos(\varphi_r)\cos(\delta)\sin(\omega_s)]$$

where

R_a : extraterrestrial radiation [MJ m^{-2} day^{-1}],

φ_d : latitude (decimal degrees)

φ_r : latitude (radians)

J : Julian day

d_r : inverse relative distance Earth-Sun

δ : solar declination

ω_s : sunset hour angle

G_{sc} : solar constant = 0.0820 [MJ m^{-2} min^{-1}],

Net outgoing longwave (R_{nl}) radiation is calculated from temperature, vapour pressure and relative shortwave radiation by:

$$R_{nl} = \sigma \left[\frac{T_{max,K} - T_{min,K}}{2}\right] [0.34 - 0.14\sqrt{e_a}] \left[1.35 \frac{R_s}{R_{s_0}} - 0.35\right]$$

Where outgoing longwave (R_{nl}) radiation is calculated from temperature, vapour pressure and relative shortwave radiation by:

R_{nl} : Net outgoing longwave radiation [MJ m^{-2} day^{-1}],

σ : Stefan-Boltzmann constant [0.4903 10^{-9} MJ K^{-4} m^{-2} day^{-1}],

$T_{max,K}$: maximum absolute temperature during the 24-hour period [K=^{o}C + 273.16],

$T_{min,K}$: minimum absolute temperature during the 24-hour period [K=^{o}C + 273.16],

e_a : actual vapour pressure [kPa],

R_s/R_{s_0} : relative shortwave radiation (limited to ≤ 1.0),

R_s : solar radiation [MJ m^{-2} day^{-1}],

Clear sky solar radiation, R_{so}, is calculated by:

$$R_{so} = (0.75 + 2 \times 10^{-5} z) R_a$$

Where z is the elevation above sea level (m). Saturation vapour pressure is related to air temperature and can be calculated using the following relationship:

$$e^o(T) = 0.611 e^{\left(\frac{17.27T}{T+237.3}\right)}$$

Where T is given in ^{o}C. In lieu of dewpoint temperature measurements, the daily minimum temperature, T_{min}, may be used estimate the actual vapour pressure using the relationship:

$$e_s = e^o(T_{min}) = 0.611\, e^{\left(\frac{17.27T_{min}}{T_{min}+237.3}\right)}$$

Similarly, mean daily saturation vapour pressure should be estimated as the mean between saturation vapour pressure at the daily maximum and minimum temperature:

$$e_s = \frac{e^o(T_{max}) + e^o(T_{min})}{2}$$

Wind speed at 2 meters is estimated from the WATCH Driving Data 21st Century wind speed at 10 m using the power low:

$$\mu_2 = \mu_z \frac{4.87}{\ln(67.8z - 5.42)}$$

Where

μ_2 : wind speed at 2 m above ground level [m s^{-1}],

μ_z : wind speed at z m above ground level [m s^{-1}] (in this case z=10 m),

Finally, the saturation-vapor-pressure vs. temperature curve at the given air temperature psychrometric constant, Δ, is calculated based on mean daily temperature (T^oC) :

$$\Delta = \frac{4098\left[0{,}6108e^{\left(\frac{17.27T}{T+237.3}\right)}\right]}{(T + 237.3)^2}$$

and the psychrometric constant γ, is calculated based on atmospheric pressure, P,

$$\gamma = \frac{1.013 \times 10^{-3} p}{0.622 \times 2.45}$$

and

$$P = 101.3\left(\frac{293 - 0.0065z}{293}\right)^{5.26}$$

4.2.2 Computation of SPEI for the control period

Another significant point of this thesis is that the three parameter Generalized Extreme Value (GEV) statistical distribution was applied for the fitting of the differences $P - PET$, instead of the Log-logistic. That was done following the recommendations which outlined in Stagge et al. (2014). So, Log-logistic distribution was not applied according to the definition of SPEI by Vicente-Serrano et al. (2010). As it is mentioned in Stagge et al. (2014) the GEV actually performs better than the Log-logistic for Europe. In addition, it has the benefit of being better understood and avoids the confusing formulation.

The formula of Generalized Extreme Value distribution is presented below

$$F(\mathrm{x}) = \begin{cases} \left(\frac{1}{\sigma}\right)(1+\xi \mathrm{z}(\mathrm{x}))^{-1/\xi - 1} \mathrm{e}^{-(1+\xi \mathrm{z}(\mathrm{x}))^{-1/\xi}}, & \xi \neq 0, 1+\xi z(x) > 0 \\ \left(\frac{1}{\sigma}\right) \mathrm{e}^{-\mathrm{z}(\mathrm{x}) - \mathrm{e}^{-\mathrm{z}(\mathrm{x})}}, & \xi = 0, -\infty < x < \infty \end{cases}$$

where

$$\mathrm{z}(\mathrm{x}) = \frac{\mathrm{x} - \mu}{\sigma}$$

μ ∈ R, σ > 0and ξ ∈ R which are the location, scale, and shape parameters

The distribution parameters were calculated according to L-moments method (Hosking 1990). The location parameter corresponds to the first L-moment λ_1, the scale parameter to the second L-moment λ_2 and the shape parameter to the L-coefficient of variation (L-CV). The $\lambda_1$and λ_2 obtained from probability-weighted moments (PWMs) using the formulas :

$$\lambda_1 = \mathrm{w_o}$$

$$\lambda_2 = \mathrm{w_o} - 2\mathrm{w_1}$$

$$t = {\lambda_2}/{\lambda_1}$$

where the PWMs of order s are calculated as:

$$\mathrm{w_s} = \frac{1}{\mathrm{N}} \sum_{\mathrm{i}=1}^{\mathrm{N}} (1 - \mathrm{F_i})^{\mathrm{S}} \mathrm{D_i}$$

where N is the number of data, F_i is a frequency estimator following the approach of Hosking (1990) and D_i is the difference between Precipitation and Potential Evapotranspiration for the day i.

With F(*x*) the SPEI can easily be obtained as the standardized values of F(*x*). For example, following the classical approximation of Abramowitz and Stegun, 1965:

$$SPEI = W - \frac{C_0 + C_1 W + C_2 W^2}{1 + d_1 W + d_2 W^2 + d_3 W^3}$$

where

$$W = -2\ln(P),$$

for $P \leq 0.5$, P being the probability of exceeding a determined D value, P=1-F(x). If $P>0.5$, P is replaced by $1-P$ and the sign of the resultant SPEI is reversed. . The constants are: $c_o = 2.515517$, $c_1 = 0.802853$, $c_2 = 0.010328$, $d_1 = 1.432788$, $d_2 = 0.189269$, $d_3 = 0.001308$.The average value of the SPEI is 0, and the standard deviation is 1. The SPEI is a standardized variable, and it can therefore be compared with other SPEI values over time and space. An SPEI of 0 indicates a value corresponding to 50% of the cumulative probability of D.

By this way, the SPEI for the control period was calculated. This procedure is followed for the outcomes of the three GCMs models.

4.2.3 Computation of SPEI for the future period

Next step is the estimation of the SPEI index for the 21st Century. The procedure is the same with the calculation of SPI for the future period. Using the distribution parameters of the control period, the probabilities of the future precipitation values are calculated. It is done based on the same formula of Generalized Extreme Value distribution as it is presented below :

$$F(x) = \begin{cases} \left(\frac{1}{\sigma}\right)(1+\xi z(x))^{-1/\xi - 1} e^{-(1+\xi z(x))^{-1/\xi}}, & \xi \neq 0, 1+\xi z(x) > 0 \\ \left(\frac{1}{\sigma}\right) e^{-z(x) - e^{-z(x)}}, & \xi = 0, -\infty < x < \infty \end{cases}$$

With F(*x*) the SPEI can easily be obtained as the standardized values of F(*x*). For example, following the classical approximation of Abramowitz and Stegun, 1965:

$$SPEI = W - \frac{C_0 + C_1 W + C_2 W^2}{1 + d_1 W + d_2 W^2 + d_3 W^3}$$

where

$$W = -2\ln(P),$$

for $P \leq 0.5$, P being the probability of exceeding a determined D value, P=1-F(x). If $P>0.5$, P is replaced by $1-P$ and the sign of the resultant SPEI is reversed. . The constants are: $c_o = 2.515517$, $c_1 = 0.802853$, $c_2 = 0.010328$, $d_1 = 1.432788$, $d_2 = 0.189269$, $d_3 = 0.001308$.

By this way, the SPEI for the control period was calculated. This procedure is followed for the outcomes of the three GCMs for all the future periods.

4.2.4 Index range limitation

At this point it should be mentioned that SPEI values are limited to the range [-3,3] to ensure reasonableness. As it is explained by Stagge et al. (2014), this issue has not been addressed explicitly in previous studies; however, the process of calculating unbounded SPI and SPEI values based on the relatively limited historical record requires significant extrapolation and the associated uncertainty.

The point is that we are using 30 years to calculate SPI of -3, which equates to an event that happens once in 740 years. So, we are already outside our original range. Events outside this range are not removed from the time series, but are designated <-3 or >3 to show that the event is extreme but cannot be accurately quantified. Placing reasonable limits on SPI and SPEI or providing uncertainty bounds is recommended for all future studies using these indices (Stagge et al., 2014).

4.3 Box plot

The boxplot is graphical display of the five-number summary (minimum, first quartile, median, third quartile and maximum) of a batch of numbers which shows much of the structure of the batch. From the boxplot we can pick out the following features of a batch: location, spread, skewness, tail length and outlying data points. Thus the boxplot provides a visual impression of several important aspects of the empirical distribution of a batch of data. All these attributes make boxplot very useful

when large numbers of observations are involved and when two or more data sets are being compared. So, the boxplot fits to the present work for both of these two reasons. That because, so, the produced values of the indices are huge tables of 9.855.000 ($270\text{cells} \times 100\text{years}$) observations for each combination of GCM-scenarios. As, because these observations are generated for 6 different combination of future data which leads to the need of comparing all these datasets.

In the following paragraph, the description of Emerson and Strernio (1983) follows, regarding to the computation and the drawing of a boxplot. According to them, the first step of the analysis is the construction the calculation of the minimum, first quartile, median, third quartile and maximum. Then the fourth-spread and the cutoffs for outliers, based on the fourth-spread, are calculated.

The fourth-spread is the range of the data defined by the upper fourth and the lower fourth quartile of the sample. It is closely related to the inter quantile range, although technical differences between quartiles and fourths distinguish the two concepts.

Data values that are far enough beyond the fourths are considered as potential outliers. The fourth-spread is used to make this vague concept precise and give technical meaning to the term of "outlier". Specifically, the $\mathrm{F_L} - \frac{3}{2}\mathrm{d_F}$ and the $\mathrm{F_U} + \frac{3}{2}\mathrm{d_F}$ are defined as the outlier cutoffs, where $\mathrm{F_L}$ and $\mathrm{F_U}$denote the fourths and $\mathrm{d_F}$ is $\mathrm{F_U} - \mathrm{F_L}$, the fourth-spread. Data values that are smaller than $\mathrm{F_L} - \frac{3}{2}\mathrm{d_F}$ or larger than $\mathrm{F_U} + \frac{3}{2}\mathrm{d_F}$ are called outliers. To construct the boxplot, we first draw a box with ends at the lower fourth and the upper fourth and a crossbar at the median. Next, we draw a line from each end of the box to the most remote point that is not an outlier.

The resulting figure schematically represents the body of data minus the outliers. The outliers are represented individually by spots situated beyond the outlier cutoffs.

The box plot shows at a glance the location, spread, skewness, tail length, and outlying data points. The location of the batch is summarized by the median, the crossbar in the interior of the box. The length of the box shows the spread, using the fourth-spread. From the relative positions of the median, the upper fourth and the lower fourth, we also see some of the skewness; e.g. when the median is much closer to the lower fourth than to the upper fourth, indicate that the batch is positively skewed. The plot indicates tail length by the extension of the lines, and by the outliers.

4.4 Empirical cumulative distribution function

In order to approach how the distribution of the indices values proceeds in the future periods, the cumulative distribution function was considered as the best way. More specifically, the empirical cumulative distribution function was chosen.

An empirical cumulative distribution function (ECDF) is a non-parametric estimator of underlying cumulative distribution function (CDF) of a random variable It assigns a probability of $1/n$ to each datum, orders the data from smallest to largest in value, and calculates the sum of the assigned probabilities up to and including each datum. The result is a step function that increases by $1/n$ to each datum[8].

The empirical cumulative distribution function is usually denoted by $\widehat{F_n}(x)$, and is defined as

$$\widehat{F_n}(x) = n^{-1} \sum_{i=1}^{n} I(x_i \leq x)$$

where $I()$ is the indicator function. It has 2 possible values: 1 if the event inside the brackets occurs, and 0 if not.

$$I(x_i \leq x) = \begin{cases} 1, & when\ x_i \leq x \\ 0, & when\ x_i > x \end{cases}$$

. The empirical cumulative distribution function fits in our case because:

- It approximates the true cumulative distribution function well if the sample size is large, which is in the present work, and knowing the distribution is helpful for statistical inference.
- a plot of the empirical cumulative distribution function can be visually compared to known cumulative distribution functions of frequently used distributions to check if the data came from one of those common distributions.
- it can visually display the ratio that the cumulative distribution function increases to 1.

This distribution covers full the needs of the present work. So, there was no need for furthermore research to another common distributions

[8] http://www.r-bloggers.com/exploratory-data-analysis-conceptual-foundations-of-empirical-cumulative-distribution-functions/

5 Results

5.1 Results of SPI

5.1.1 Parallel Boxplots of SPI values

After the analysis according to the methodology section, all the SPI and SPEI values for all the combination of GCM-Scenario are available. Then, the first and basic step, after the creation of the drought indices, is to make a boxplot which is a standardized way of displaying the distribution of data.

Especially, figure 6, presents parallel boxplots. By this way, datasets from several distributions are displayed on the same chart, using the same measurement scale.

In figure 6, the vertical axis, which is the main axis of a boxplot, indicates the SPI values. The horizontal axis indicates the several time periods. As it seems, there are 4 different time periods. One which corresponds to the control period (1961-1990) and three which correspond to future periods (2011-2040, 2041-2070 and 2071-2100). Regarding to that, even if the whole future period corresponds to 100 years (21st Century), it was split up in three 30-years time periods. This classifications gives so higher accuracy in the interpretation of the droughts as reveals the temporal variability of the indices in the 21st Century. Furthermore, by this way, the length of the control period and the futures period is the same. That fact makes possible the comparison between these the several time periods.

In the same figure (Figure 6), we observe that 3 boxplots exist for the control period and 6 boxplots for each future period. That happens because each boxplot concerning the control period represents the SPI values as they arose from the analysis of the outputs of each GCM. These results are based on the past data, so there is no scenario for the past, so 3 GCMs produce 3 boxplots. In the contrary, 6 boxplots are presented for each of future period. That happens because two datasets, one for each scenario (A2 and B1), are recreated for each GCM. So, 3 GCMs and two scenarios gives 6 boxplots. More details, regarding to which boxplot correspond to each GCM and scenario, are given in the legend of the Figure 6.

It should be remarked that each time period, so the control (1961-1990) as the future (2011-2040, 2041-2070 and 2071-2100) periods has got 30-years length. In addition, the land of Greece corresponds to 270 cells of the half degree grid. That fact means that each boxplot represents $270 cells \times 365 \text{days} \times 30 \text{years} = 2{,}956{,}500$ SPI values.

The next part of the present subsection refers to the presentation of the results. Due to the fact that there are 4 time periods, 3 models and 2 scenarios, all comments organized as it is illustrated below. Firstly, the control period is depicted. Secondly, the behavior of each GCM for a certain scenario is cited. In details, the results of each model for a certain scenario and for the several future periods are illustrated. Secondly, a comparison between the two scenarios is done. And ,finally, the comparison between the GCMs is done, also.

The boxplots of control period present similarities between the several models. The similarities correspond to the median, the first and third quantile. The median is close to zero as it was expected because of the standardization. Based on the same reason, the median looks that keeps similar distances from the first and the third quantile in each case. That declare that there is no significant skewness in the SPI values. That is valid for all the GCMs. But, the first and third quantile present similar values for all the models, also. The ECHAM model presents shorter range between the first and the third quantile (interquantile range, IQR), but it remains still close to the other models. The range between the first and the third quantile is called interquantile range (IQR). All that mean, that all the models are in agreement in the control period regarding to these characteristics (median and IQR).

The presentation of the results of B1 scenario periods is the next issue . In the first future period (2011-2040), the IQR and the median of SPI values of the ECHAM model are slightly shifted to more positive values. More positive values means wetter conditions and more negative values defines drier conditions. The IQR of the same model presents a weak expansion. The median still remains in the middle of the box, which means no significant skewness of the data. IPSL IQR remain in the same level with the control period but it is shrunk and with a slight skewness to the lower values of SPI according to the median. On the other hand, the IQR of CNCM3 presents a stronger shift to drier conditions and its more spread than the other two. Furthermore, a slight skewness to lower values is presented by this model. The second future period (1941-1970) the CNCM3 presents a shrinking of the IQR, without presence of shift and skewness. The two other models present a shift to drier conditions. After that, all the model are in agreement for this period, with similar IQR and median. In the last future period (2071-2100), no significant differences in the median and IQR for the IPSL and ECHAM models are presented, just small deviations from the previous time period. Finally, the boxplot of CNCM3 model denotes a strong shift to extreme dry conditions, expansion of the IQR and high skewness to the lower values.

The A2 scenario gives more complex results. In the first future period (2011-2040), ECHAM model describes a similar climate with the control period. The median

remains close to 0. That fact means equal number of dry and wet days in comparison with the control period. The unique difference is that the values of both, dry and wet days, are more expanded. CNCM3 and IPSL models illustrate similar condition for this period. They are shifted to drier conditions and they present a skewness to the lower SPI values. Wet conditions, in comparison with the control period, are existed over the third quantile. The next period (1941-1970) the ECHAM and IPSL IQRs present a shift to lower SPI values. In this period, in contrast with the previous, the ECHAM IQR presents a strong shift to drier conditions, whilst IPSL shows a softer shift. The result is that both models are in the same level in this period, with the IQR of ECHAM to be more spread. The CNCM3 IQR presents a shift to lower SPI values, which is the same with the shift of the previous time period. The IQR is significantly spread in comparison with the IQR of the previous time period. Finally, in the last period (1971-2100), the differences between the models are more obvious. The IQR of all the models are spread in comparison with the period 1941-1970. In addition, significant shifts to drier conditions are presented. And the skewness of the data varies between the models.

According to the boxplots of A2 scenario, the ECHAM shows the lower deviation of SPI values from the control period. ECHAM follows with intermediate deviation between the three. And, finally, CNCM3 presents the higher deviation from the other two models. This pattern is repeated in each future period for the A2 scenario. In contrast, there is no steady pattern for the results of B1 scenario. Despite that fact, in the case of B1 scenario, the results of SPI from the three models remain closer each other.

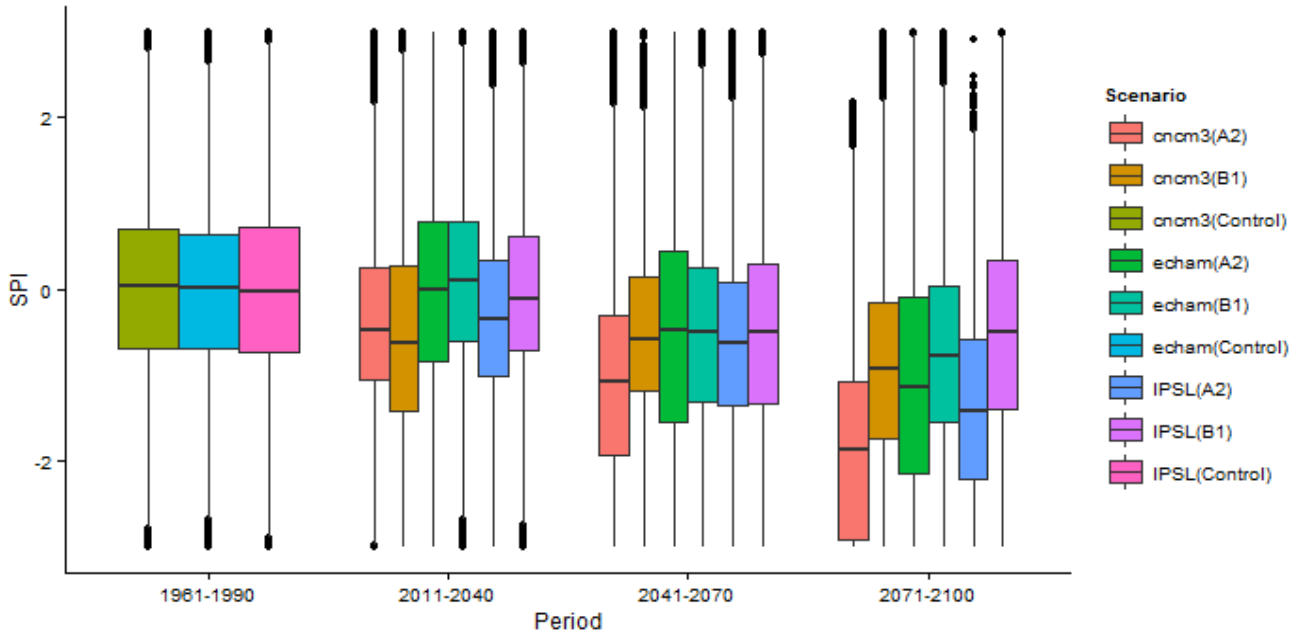

Figure 6: SPI boxplots. The first time period (1961-1990) corresponds to the results of the GCMs for control period. The first one correspond to CNCM3, the second one to ECHAM and the third one to IPSL. The rest time periods (2011-2040, 2041-2070, 2071-2100) correspond to the future periods. To each future period, the first two boxplots correspond to CNCM3, the second two correspond to ECHAM and the third two correspond to IPSL. For each pair now, the left boxplot corresponds to the A2 scenario and the right boxplot to the B1 scenario.

5.1.2 Empirical cumulative distribution functions of SPI

Afterwards, the empirical cumulative distribution functions (ecdf), of each time period and each combination of GCM-Scenario, are presented. The multiple plot figure, figure 7, illustrates all these empirical cumulative distributions functions. Figure 7 consists in 2 rows and 3 columns. The two rows refer to the selected scenarios which are A2 and B1 in our case, whilst the three columns indicate the relevant GCMs.

Additionally, the theoretical normal distribution of the control period is plotted. It is done in order to visualize the difference between the theoretical and the empirical distribution functions for the control period. Generally, we do not expect differences between them because the empirical distribution is based on the standardized gamma distribution into a normal. Nevertheless, a differentiation exists because of the limitation of the index range [-3,3] but in our case it is assumed negligible.

Afterwards, the results of ECDF plots are described. The description of the results are based on the time period and the scenario. For example, initially, the ECDFs of 2011-2041 period for each model for B1 scenario are presented, and the next periods follow. So the differences and similarities between the 3 models are mentioned, as the differences and similarities between ECDF of the previous time periods.

At first, the control period is commented. The ECDF of control period is the for both scenarios. That means that the red lines for both plots which correspond to ECHAM model represent the same SPI values, because as it aforementioned above the data for the control period is unique, there is no existence of scenarios.

The presentation of the results of the first future period (2011-2040) and B1 scenario follow. It should be notice again that the time space between the control period is 20 years (1991-2010). It is important to be clear for the understanding of the results. The ECHAM and IPSL ECDF for this period present similar patterns with the ECDF of the control period. The ECDF of ECHAM is slight shifted to higher values of SPI, whilst the one of IPSL is slight shifted to lower values. But, nevertheless, the patterns remain quite similar. The ECDF of CNCM3 presents so a relatively strong shift to more negative values, as an increased ratio from 0 to 1

cumulative probability. In the next future period (2041-2070) CNCM3 ECDF remains in the same level but with a lower ratio than in the previous period. In this future period, ECDF of IPSL and ECHAM presents a shift to more negative values, which is similar of the previous shift of CNCM3. In this period, all the ECDFs are in the same level. Nevertheless, the ratios vary. It should be marked that the negative tails of IPSL and ECHAM ECDFs don't start from zero value. It 's matter of the limitation of the index range and it is discussed in the section of Discussion. Finally, in the last future period (2071-2100), the ECHAM and CNCM3 ECDFs present shift to more negative values again. On the other, the IPSL ECDF follows similar patterns as in the previous future period.

Subsequently, the A2 scenario is outlined. Generally, stronger shifts, higher diversity on the ratios and more obvious the effect of the index range limitation characterize this scenario, in comparison with the B1. The ECDFs of control period are the same as before, so no more comments on these follow. In the first future period (2011-2040), CNCM3 ECDF presents higher so higher ratio as a shift to more negative values of SPI. The ECHAM ECDF remain in the same level with the control period but with lower ratio and smoother tails in the extremes. And, finally, the IPSL ECDF present A shift to more negative values with similar positive tail and smoother negative than before. In the next future period (2041-2070) all the ECDFs present shift to more negative values, with shifts of CNCM3 and ECHAM being stronger than the one of IPSL. The effect of limitation of the index range get more significant for CNCM3 and ECHAM. The negative tails tends to disappear. The positive tail of CNCM3 longer while the one of ECHAM smoother. The ECDF of IPSL present a shift to more negative values with shorter negative tail and longer positive tail. Eventually, in the last future period (2071-2100), gets stronger to each ECDF with almost no negative tails and prolonged positive tails.

Concluded, some comments regarding to the differences between A2 and B1 scenarios could be mentioned. Firstly, the ECDFs of A2 scenario expand to more negative values along the time than the ECDFs of B1 scenario. In addition, the effect of the limitation of the index range is stronger in A2 scenario. Finally, the positive tails get longer, whilst the negative shorter and smoother.

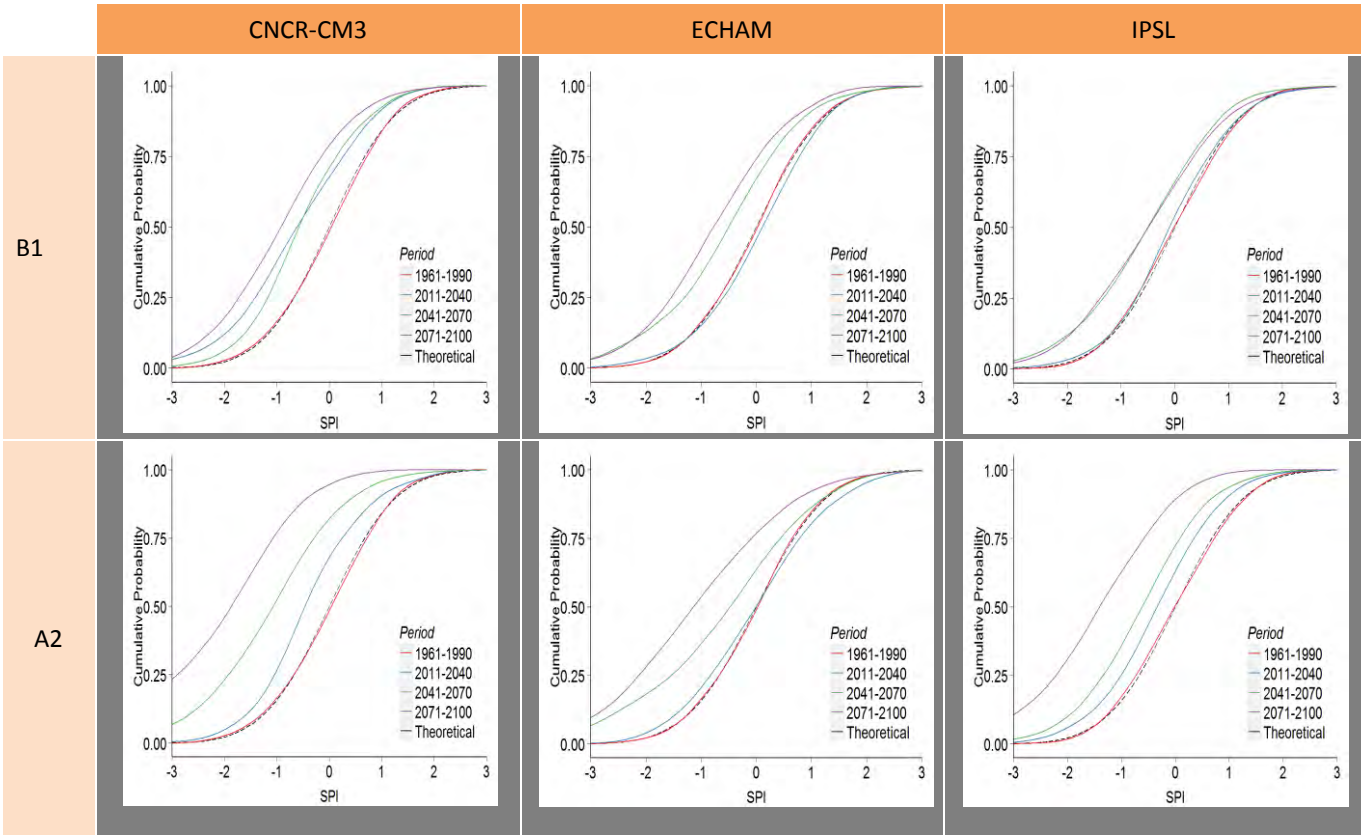

Figure 7: SPI ECDFs. The broken line presents the theoretical normal distribution, while the red, blue, green and purple lines present the control period 1961-1990 and the future periods 2011-2040, 2041-2070 and 2071-2100, respectively. The three columns correspond to the GCMs and the two rows to the emission scenarios.

5.2 Results of SPEI

5.2.1 Parallel Boxplots of SPI values

In this subsection, the boxplots concerning the SPEI results are represented. The arrange and the structure of figure 8 follow the same pattern as it described in the respective subsection 5.1.1 of SPI results.

The rest of this subsection refers to the presentation of the results. Firstly, the control period is depicted. Secondly, the behavior of each GCM for a certain scenario is cited. In details, the results of each model for a certain scenario and for the several future periods are illustrated. Secondly, a comparison between the two scenarios is done. And ,finally, the comparison between the GCMs is done.

Originally, the boxplots of the SPEI values for the control period are outlined (Figure 8). There are no significant differences among the boxplots of the SPEI values for the several GCMs. The median and the IQR show similar values with small fluctuations.

Consequently, the B1 scenario is described (Figure 8). In the first future period (2011-2040), IQR of the ECHAM is slightly moved to drier conditions . The median remains close to 0. So, the data presents a skewness to the positive values of SPEI. The IPSL IQR is shifted to lower values and present a skewness to more negative values. On the other hand, CNCME3 presents the strongest shift to drier conditions and a significant expansion of the IQR. In addition, its median is closer to the fist quantile that fact denotes a skewness of the SPEI values to lower values. In the second future period (2041-2070), the median of CNCM3 does not show significant change, the skewness remains and the IQR shrinks. Median and IQR of ECHAM and IPSL shift together to the same level of CNCM3, but in contrast with CNCM3, their IQR expand instead of shrinking. The median is similar for all models in this period. Finally, in the last future period (2071-2100), the boxplots of the three models move parallel to more negative values. The shifts of CNCM3 and ECHAM are similar and higher than the shift of IPSL. Their IQR is additionally expanded for all of them.

Afterwards, the results of the A2 scenario are illustrated. The first future period (2011-2040), the third quantile and the median of ECHAM are maintained in the same level with the control period. The values between the median and the first quantile of the same model expand. The IPSL and CNCM3 IQR present a strong similar shift to more negative values. The next future period (2041-2070), All the models present a significant expansion of the IQR and strong shift to more negative values. A slight skewness to more positive values it is shown for all of them. Finally, in the last future period (2071-2100) the effect of index range limitation is obvious for all the models. the results show strong shifts for all of them and high skewness to extreme drought conditions. The IQR shrinks due to the index range limitation.

According to the boxplots of A2 scenario, the ECHAM shows the lower deviation of SPI values from the control period. ECHAM follows with intermediate deviation between the three. And, finally, CNCM3 presents the higher deviation from the other two models. This pattern is repeated in each future period for the A2 scenario. In contrast, there is no steady pattern for the results of B1 scenario. Despite that fact, in the case of B1 scenario, the results of SPI from the three models remain closer each other.

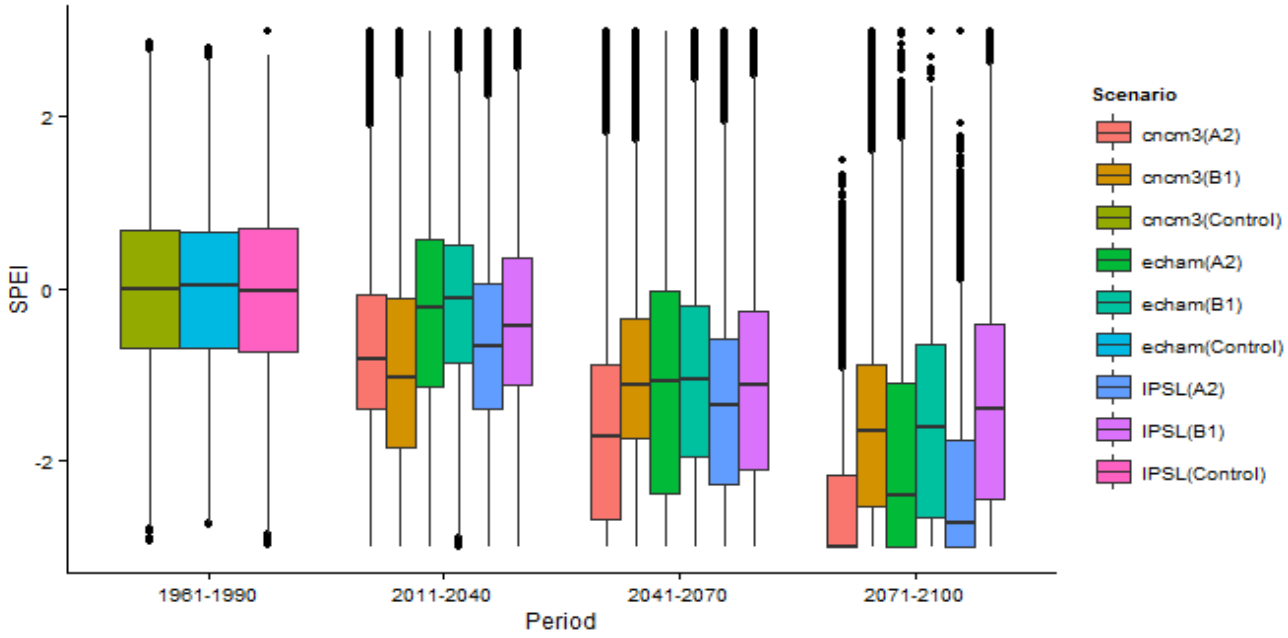

Figure 8: SPEI boxplots. The first time period (1961-1990) corresponds to the results of the GCMs for control period. The first one correspond to CNCM3, the second one to ECHAM and the third one to IPSL. The rest time periods (2011-2040, 2041-2070, 2071-2100) correspond to the future periods. To each future period, the first two boxplots correspond to CNCM3, the second two correspond to ECHAM and the third two correspond to IPSL. For each pair now, the left boxplot corresponds to the A2 scenario and the right boxplot to the B1 scenario.

5.2.2 Empirical cumulative distribution functions of SPEI

Afterwards, the empirical cumulative distribution functions (ecdf), of each time period and each combination of GCM-Scenario, are illustrated. But, now, figure 9 features the SPEI values, instead of SPI values. The way is the same. The multiple plot figure, figure 9, consists in 2 rows and 3 columns, again. The two rows refer to the selected scenarios which are A2 and B1 in our case, whilst the three columns indicate the relevant GCMs.

Additionally, the theoretical normal distribution of the control period is captured. It is done in order to visualize the difference between the theoretical and the empirical distribution functions for the control period. Generally, we do not expect differences between them because the empirical distribution is based on the standardized gamma distribution into a normal. Nevertheless, a differentiation exists because of the limitation of the index range [-3,3] but in our case it is assumed negligible.

Afterwards, the results of ECDF plots are described. The description of the is based on the time period and the scenario. For example, initially, the ECDF of 2011-2041 period for each model for B1 scenario is presented, and the next follow. So

the differences and similarities between the 3 models are mentioned, as the differences and similarities between ECDF of the previous time periods.

The ECDF of SPEI values for the B1 scenario are shown below. The influence of index value limitation is obvious from the first future period for the CNCM3 model. A strong shift to more negative values, no tail in the negative SPEI values, longer tail in the positive values and lower ration of increase for the cumulative probability characterize this ECDF. The ECHAM ECDF presents a weak shift to more negative values. The only difference in the shape of the curve in comparison with the respective curve of the control period is the less smooth tails for the positive SPEI values. The IPSL ECDF present shift to more negative values, also. The difference between the shape of the ECDF of the control period is that the curve is smoother for the positive values. In the next future period (2041-2070), the effect of index limitation start to be obvious for all GCMs. The results of CNCM3 ECDF don't show any shift but the present a steeper increase of the cumulative probability. In contrast, the ECHAM an IPSL indicate strong shift to more negative values. Both curves present similar patterns, with no tail in the negative values of SPEI and long tail in the positive values. All the models follow the same pattern the next future period (2071-2100) but moved to more negative values.

Consequently, the results for the A2 scenario are illustrated. In the first future period (2011-2040), the ECHAM ECDF shows strong shift two more negative values of SPEI. The tail of the lower SPEI values is shorter than in the control period while the tail of the higher SPEI values is smoother and longer in comparison with the control period. The ECDF of ECHAM shows smoother shape for until the 0.5 cumulative probability in comparison with the control period whilst keep the same shape above this value. Finally, the IPSL ECHAM shows a shift to more negative values without significant changes on the shape of the curve. No tails for the lower values, long tails for the higher and differences in the ratio characterize the ECDFs of the second future period. Eventually, the last future period (2071-2100) show extreme negative values. Similar pattern indicate that around the half data has got -3 value in all the cases. Moreover, there are no values over the 0 SPEI value. Exception is the ECHAM in which some positive value remain.

Generally, the results the SPEI reveal very strong shifts between the several periods. And the shifts are much stronger than the shifts of SPI. Furthermore, the shifts in B1 scenario are weaker than the shifts in A2 scenario. Additionally, the use of the index range limitation plays determinant role in the final shape of the ECDFs.

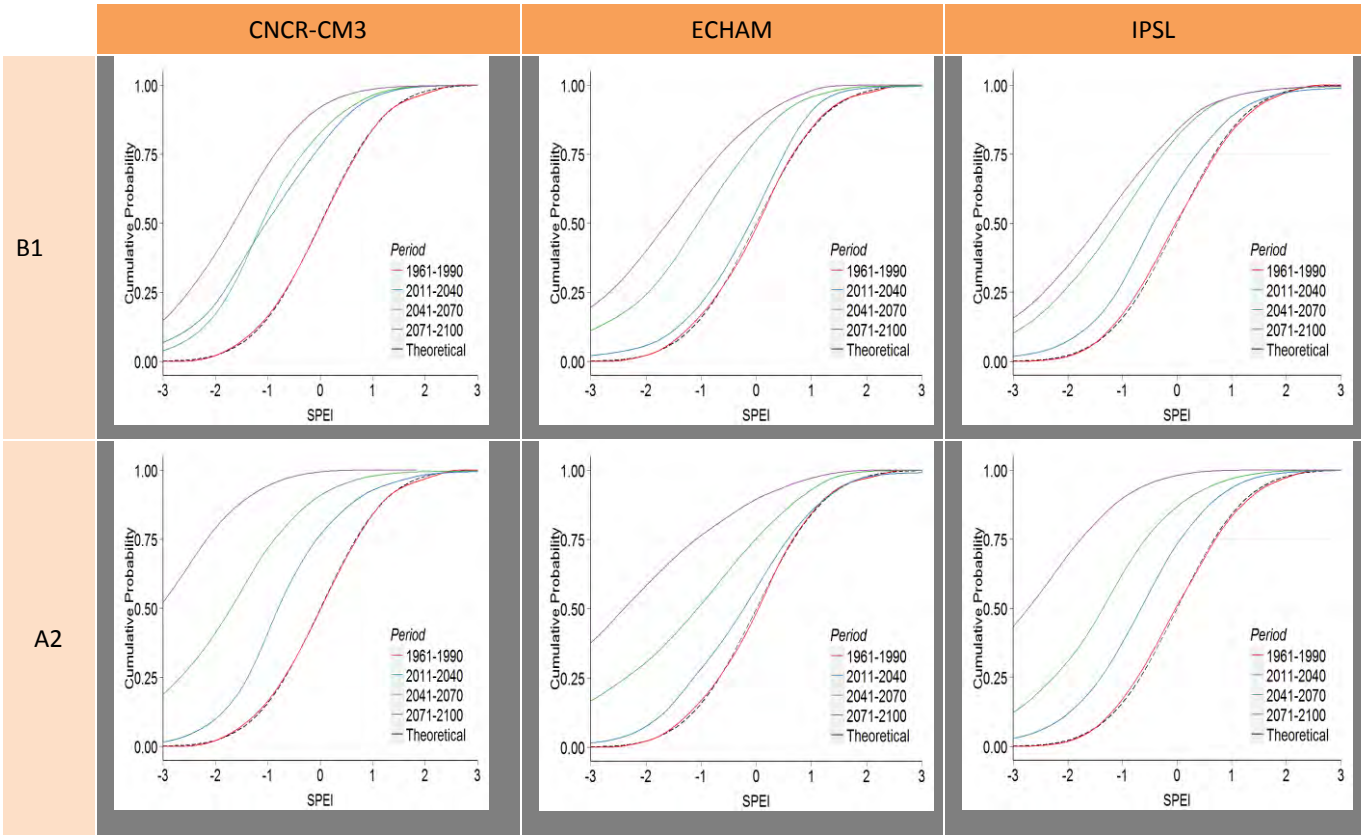

Figure 9: SPEI ECDFs. The broken line presents the theoretical normal distribution, while the red, blue, green and purple lines present the control period 1961-1990 and the future periods 2011-2040, 2041-2070 and 2071-2100, respectively. The three columns correspond to the GCMs and the two rows to the emission scenarios.

6 Discussion

6.1 B1 and A2 scenarios

As it was described in subsection 2.4.2, B1 future climate scenario represents a convergent world with the same global population, rapid changes in economic structures toward a service and information economy, reductions in material intensity and the introduction of clean and resource-efficient technologies. On the other hand, A2 scenario Illustrates a very heterogeneous world with continuously increasing global population and regionally orientated economic growth. These assumptions lead to different greenhouse gas emissions which, consequently, affect the climate. Based on these assumptions the greenhouse gas emissions play significant role in the formation of the future climate. As higher are the emissions sobigger are the changes in the future climate.

Generally, B1 scenario considers a future world close to the current world. On the contrary, A2 scenario assume an increasing global population and not well

organized. That fact mirrors to the outcomes of the several GCMs. The outcomes of GCMs present higher decrease of precipitation and higher increase of temperature for the A2 scenario that for the B1. Deeper explanation, based on the natural processes and the way with which the GCMs regenerate them, wanders from the topic of the present thesis

So, based on the decrease of the precipitation in the future, the decreased value of SPI can be explained. Initially, if we simplify the SPI, as the deviation of the precipitation values from the mean precipitation. For the control period, drought conditions are defined the negative deviation of precipitation values from the mean precipitation of the same period. For the future period, SPI was defined as the negative deviation of the precipitation values from the mean precipitation of the control period. Hence, as the precipitation values decrease in the future, these values correspond to more negative deviations from the mean precipitation of the control period. A2 scenario gives, generally, lower precipitation values than the B1 scenario, as it arises from the outcomes of the several GCMs. That fact interprets why the A2 scenario presents lowers SPI values than the B1 scenario .

In similar fashion, the lower values of A2 scenario than B1 scenario are interpreted for the case of SPEI index. But because the SPEI is based on the water balance $P - PET$, some points should be mentioned. In this case, both precipitation and evapotranspiration change along the time. More specifically, the precipitation values decrease and the potential evapotranspiration values increase. Both cases lead to lower values of the difference $d = P - PET$ in reference to the control period. Consequently, that fact leads to higher negative deviation from the mean differences of the control period. Related to the two scenarios, A2 scenario describes a future climate with less precipitation, higher temperature and higher evapotranspiration than B1 scenario. That fact leads to more extreme values of SPEI for A2 scenario. More details regarding to the future proportion of P and PET are given in the next 6.2 subsection concerning the comparison between the SPI and SPEI.

6.2 SPI and SPEI

SPI and SPEI drought indices present significant differences regarding to the evolution of droughts in the 21st Century. Both indices indicate drier conditions for the future. That was expected for both indices based on the signs of the GCMs outcomes regarding to decreased precipitation, increased temperature, increased evapotranspiration etc. Nevertheless, SPEI index presents more intense droughts than SPI.

The main cause for the difference between the two indices is that the indices are based on different variables. SPI is generated from precipitation values and SPEI is produced from the differences $P - PET$. So, potential evapotranspiration is the determinant element which defines this difference between the two indices. Actually, the precipitation variable is common for both indices, while the potential evapotranspiration concerns the SPEI. The potential evapotranspiration increases along the time, according to the outcomes of GCMs. That fact explains why SPEI presents lower values than SPI.

In case of SPI, it is clear that the lower future precipitation values present negative deviation from the mean precipitation of the control period. About SPEI, the increased future potential evapotranspiration makes the gap (deviation) between the values of the differences $d = P - PET$ of future periods and the mean of the control period higher between the gap of precipitation between the same periods. Concluded, the increased potential evapotranspiration is responsible for the difference between the two indices.

6.3 Index range limitation

The effect of index range limitation between [-3,3] is obvious in all the 30 years future periods. As it seems in boxplots, it concerns big part of values under the first quantile the two first future periods, 2011-2040 and 2041-2070, respectively, whilst bounds noticeable the interquantile range of SPEI values the last future period (2071-2100). That happens because big amount of the lowest values of precipitation and $\mathrm{P} - \mathrm{PET}$ of the SPI and SPEI of future, respectively, correspond to lower than values -3 of SPI and SPEI of the control period. The real values of the indices for these values hide high uncertainty. That because they are so extreme for the control period and present many times higher return period than the 30 years length of the control period. So, in case of avoiding wrong interpretation of the results, they are assumed extreme events without precise values. In addition, any analysis of drought severity, based on these results, should be avoided.

6.4 Interquantile range (IQR)

Another significant point, which arises from the results, is the variability of the interquantile range (IQR). The boxplots of SPI and SPEI show that IQR either expands or shrinks or remains in similar levels, without follows steady pattern, in the several future periods. It's clear from the results that the shifts of IQR to lower

Indices values illustrate a drier future under drought condition. Nonetheless, the variability of the IQR denotes something additional for the climate.

Before the explanation, it should be noticed again, that generally the IQR of the future periods is either larger or equal in comparison with the IQR of the control period. Nevertheless, exist some cases, especially, in the first future period (2011-2040), in which the IQR is shrunk and get smaller than in the control period (e.g. IQR of SPI for A2 scenario of CNCM3 GCM for the period 2011-2040 (figure 6)). But the next two period the expansion of IQR gets more and more obvious.

All that are mentioned because this change describes new climate conditions which, consequently, affect the human life. Overall, the shrinking of IQR means that the climate gets more stable, with smaller deviations from the mean conditions. On the other hand, the expansion of the IQR denotes a climate with high variability. The large interquantile range implies big gap between the drier and the wetter days.

The selected way, for the creation of the indices for the future period, does not help to define drought or wet in the future periods. But we can safely export the below conclusions for the future climate of Greece area. A not only drier climate is expected for the future but with high variability also. This variability looks to get stronger and stronger in the future.

6.5 Evolution of droughts

Generally, the outcomes of the three GCMs present a drier climate under extreme drought conditions in comparison with the climate of the control period. Nonetheless, the separation of the 21st Century into 3 30-years period showed that the evolution of drought along the time is described by different way between the several GCMs. More specifically, the time of the big changes is different. Some, happen continuously, some happen in mid-century, some at start and then stop. In addition, this changes vary between the indices and the scenarios.

Firstly, the changes in SPI are compared. The CNCM3 model presents a gradually change of SPI between the several period for the A2 scenario while the big change happens in the end of the Century for the B1 scenario. The ECHAM for A2 scenario illustrates a steady climate until the mid-century. Then the climate starts to get drier until the end of the century. B1 scenario of the same model shows a more stable climate. There is a gap between the first and the second future period, but any significant change is observed before and after these periods. The B1 scenario of IPSL presents similar characteristics with the ECHAM for the B1 scenario. While the decrease of SPI is continuously for A2 scenario of IPSL model.

The changes in SPEI follow more or less the same patterns with SPI. The difference between the SPI and SPEI is the potential evapotranspiration. That fact makes the SPEI more sensitive than SPI. So, even if the changes happen the same time they are more intense in case of SPEI. Furthermore, the when the changes was continuously in SPI, they remain continuously but with steeper slopes of decreasing in SPEI. Finally, the steady periods are replaced with small changes.

7 Conclusions

The present thesis provides the SPI and SPEI drought indices for the wider area of Greece for the 21st Century. The analysis used the outcomes of three GCMs and for two future climate scenarios , as they arisen from the WATCH project. The most significant issue of this thesis is, that the procedure of drought indices computation was modified in order to be the indices values comparable with the correspond values of the control period.

After the analysis, the results showed that the climate of Greece will become drier and drier during the 21st Century. More specifically, the droughts will be more intense and frequent in comparison with the control period. Except of that, the future climate will be more variable, as concerns droughts. The gap between the driest and the wettest days will increase. In addition, there is high uncertainty, for the extreme drought event of the future The fact that the control period lasts 30 years and the big changes in the future, don't allow us define with security the extreme drought events with index value less -3.

Another important point of this thesis is that provides a programming tool to compute the SPI and SPEI for all the available data of the WATCH project, and not only. The same analysis could be done either for the whole world or for a specific region.

Finally, the results of the SPI and SPEI could be used for furthermore analysis. Having all this data (SPI and SPEI for the 21st Century), several characteristics of droughts could be investigated. For example the severity, the intense and the duration of the drought events. Moreover, the generated index values could be used for a stochastic approach of droughts.

ANNEX A: The drought impacts in Greece according to literature research for the purpose of the present thesis.

Drought Event	Country	Start Date	End Date	Impact	Impact category	Impact Description	NUTS 1	NUTS 2	NUTS 3	References
1999-2001	Ellada	09/08/2001		7.1	Local water supply shortage/problems -drying up of local springs/wells	Danger of complete drying up of the local springs. Shortage of groundwater for agriculture use due to overexploitation from the drillings.	Kentriki Ellada	Voiotia		http://www.kathimerini.gr/97968/article/epikairothta/ellada/ligosta-ta-ydatina-apo8emata-ston-orxomeno
2000-2002	Ellada	2000	2002	2.5	Increased dieback of trees (please specify tree species in the description field!)	3.5%, 4.9% & 5.9% of dead firs the years of 2000, 2001 & 2002, respectively.	Kentriki Ellada	Anatoliki Attiki	Parnitha	http://www.kathimerini.gr/157567/article/epikairothta/ellada/ta-elata-pe8ainoyn-sthn-parnh8a
1988-1989	Ellada	1988	1989	2.5	Increased dieback of trees (please specify tree species in the description field!)		Kentriki Ellada	Anatoliki Attiki	Parnitha	http://www.kathimerini.gr/157567/article/epikairothta/ellada/ta-elata-pe8ainoyn-sthn-parnh8a
2007	Ellada	Jul-07	Jul-07	4.1	Reduced hydropower production	A week with frequent power cuts at several region of the country.	Ellada			http://www.kathimerini.gr/293685/article/epikairothta/ellada/se-katastash-synagermoy-kai-ton-aygoysto-h-deh
2007	Ellada	Oct-07		8.8	Problems with drinking water quality	Deterioration of the taste and the smell of the drinking water, but no with the microbial load.	Kentriki Ellada	Thessalia	Karditsa	http://www.kathimerini.gr/300815/article/epikairothta/ellada/kleinoyn-th-myth-toys-gia-na-pioyn-nero
2007	Ellada	Oct-07		10.1	Increased species mortality (specify species (latin term) and state whether a rare / endangered / protected species is concerned	50 member of the endangered spicies Capra aegagrus cretica, of a total population of 700 members, died while the rest survived after human action.	Nisia Aigaiou	Kyklades	Antimilos, island	http://www.kathimerini.gr/302557/article/epikairothta/ellada/elikoptero-kai-limenikoi-eswsan-toys-aigagroys
2008	Ellada	Aug-08		11.2	Structural damage to private property due to soil subsidence/shrinkage	Gaps in houses due to the prolonged drought	Voreia Ellada	Thessalia	Pinios, river	http://www.kathimerini.gr/330993/article/epikairothta/ellada/h-8essalia-sto-eleos-ths-leiyydrias
2008	Ellada	Aug-08		10.8	Lack of feed / water for terrestrial wildlife		Voreia Ellada	Thessalia	Pinios, river	http://www.kathimerini.gr/330993/article/epikairothta/ellada/h-8essalia-sto-eleos-ths-leiyydrias
2008	Ellada	Aug-08		7.6	other	The drying up of the two closer dams created problems in water supply and the irrigation of the	Voreia Elladaa	Thessalia	Pinios, river	http://www.kathimerini.gr/330993/article/epikairothta/ellada/h-8essalia-sto-

						region. Specifically, the volume of water of Plastira kai Smokovo dams this year was 60 & 22 millions cubic meters,while the mean annual volume is 133 & 105, respectively.				eleos-ths-leiyydrias
2008	Ellada	Aug-08		8.2	(Temporary) water quality deterioration/problems of surface waters (natural & manmade); e.g. significant change of physio-chemical indicators, increased concentrations of pollutants, decreased oxygen	Increaced concentrations of pollutants because of the water decreaase.	Voreia Ellada	Thessalia	Pinios, river	http://www.kathimerini.gr/330993/article/epikairothta/ellada/h-8essalia-sto-eleos-ths-leiyydrias
1958	Ellada	20/08/1958	########	14.3	Excess mortality during heat waves.	A heat wave of 7 days in Larissa and Trikala cost the life of about 600 people.	Voreia Ellada	Thessalia	Larissa and Trikala	http://www.kathimerini.gr/766599/article/epikairothta/ellada/akraia-fainomena-rekor
1987	Ellada	19/07/1987	########	14.3	Excess mortality during heat waves.	About 4000 people, just in Lekanopedio Attikis, lost their lifes because of the heat wave.	Kentriki Ellada	Attiki	Attiki Cirque	http://www.kathimerini.gr/766599/article/epikairothta/ellada/akraia-fainomena-rekor
2007	Ellada	23/06/2007	########	12.4	Other	Great part of the national park of Parnitha burned these days.	Kentriki Ellada	Attiki	Parnitha	http://www.kathimerini.gr/766599/article/epikairothta/ellada/akraia-fainomena-rekor
2007	Ellada	May-07	Aug-07	12.4	Other	A combination of increased area, and increased wildfires in number and severuty. About 2.700 km2 burned area, at least 63 fatalities, 1500 bured houses, 6000 homeless, 5 billions damages, 4.5 millions olives trees and 60000 stock burned.	Ellada			http://el.wikipedia.org/wiki/%CE%94%CE%B1%CF%83%CE%B9%CE%BA%CE%AD%CF%82_%CF%80%CF%85%CF%81%CE%BA%CE%B1%CE%B3%CE%B9%CE%AD%CF%82_%CF%83%CF%84%CE%B7%CE%BD_%CE%95%CE%BB%CE%BB%CE%AC%CE%B4%CE%B1_%CF%84%CE%BF_2007
1992-1993	Ellada	1992	1993	7.6	Other	The storage capacity of the water supply in Athens was 32 days.	Kentriki Ellada	Attiki	Athens	http://www.tovima.gr/culture/article/?aid=127851

ANNEX B: Classification of drought impacts according to EDII.

Impact Category	Impact Type and ID	Explanation
Agriculture and Livestock farming	1.1	Reduced productivity of annual crop cultivation: crop losses, damage to crop quality or crop failure due to dieback, premature ripening, drought-induced pest infestations or diseases etc
	1.2	Reduced productivity of permanent crop cultivation
	1.3	Reduction of cultivated areas due to a lack of irrigation water
	1.4	Reduced productivity of livestock farming (e.g. reduced yields or quality of milk, reduced stock weights)
	1.5	Forced reduction of stock (early selling/slaughtering)
	1.6	other
	1.7	Regional shortage of feed/water for livestock
	1.8	Increased costs / economic losses
Forestry	2.1	Reduced tree growth and vitality
	2.2	Decrease in annual non-timber products from forest trees (e.g. cork, pine nuts, etc) (please specify which kind of product
	2.3	Increased occurrence of water stress indicators and damage symptoms (e.g. premature ripening, seasoning checks, defoliation, worsened crown conditions etc.) (please specify forest type/ tree species in the description field!)
	2.4	Increase of pest / disease attacks on trees (please specify species in the description field!)
	2.5	Increased dieback of trees (please specify tree species in the description field!)
	2.6	Increased dieback of trees (please specify tree species in the description field!)
	2.7	Damage to short rotation forestry plantations (energy forestry)
	2.8	other
	2.9	Increased costs / economic losse
Freshwater Aquaculture and Fisheries	3.1	Reduced (freshwater) fishery production (please specify fish species in the description field)
	3.2	Reduced aquaculture production (please specify fish species in the description field)
	3.3	other
	3.4	Increased costs / economic losses
Energy and Industry	4.1	Reduced hydropower production
	4.2	Impaired production/shut down of thermal/nuclear power plants(due to lack of process water and/or environmental legislation/restrictions for discharges into streams)
	4.3	Restriction / disruption of industrial production process (due to a lack of process water and/or environmental legislation/restrictions for discharges into

		streams)
	4.4	other
	4.5	Increased costs / economic losses
Waterborne transportation	5.1	Impaired navigability of streams (reduction of load, increased need of interim storage of goods at ports)
	5.2	Stream closed for navigation
	5.3	other
	5.4	Increased costs / economic losses
Tourism and recreation	6.1	Reduced number of short-stay-tourists
	6.2	Reduced number of long-stay-tourists
	6.3	Sport/ recreation facilities affected by a lack of water
	6.4	Impaired use/navigability of surface waters for water sport activities (including bans)
	6.5	other
	6.6	Increased costs / economic losses
Water supply/water industries	7.1	Local water supply shortage/problems -drying up of local springs/wells
	7.2	Regional/region -wide water supply shortage/problems
	7.3	Drying up of reservoirs
	7.4	Limitations in water supply to households in rural areas (including bans on domestic water use, supply cuts, need to ensure water supply by means of water transfers or bottled water)
	7.5	Limitations in water supply to households in urban areas (including bans on domestic water use, supply cuts, need to ensure water supply by means of water transfers or bottled water)
	7.6	other
	7.7	Increased costs / economic losses
Water quality	8.1	Increased temperature in surface waters (close to or exceeding critical values)
	8.2	(Temporary) water quality deterioration/problems of surface waters (natural & manmade); e.g. significant change of physio-chemical indicators, increased concentrations of pollutants, decreased oxygen saturation levels, eutrophication, algal bloom)
	8.3	(Temporary) impairment of ecological status of surface waters (according to EU Water Framework Directive)
	8.4	(Temporary) impairment of chemical status of surface waters (according to EU Water Framework Directive)
	8.5	Increased salinity of surface waters (saltwater intrusion and estuarine effects)
	8.6	Problems with groundwater quality
	8.7	Increased salinity of water
	8.8	Problems with drinking water quality (e.g., increased treatment, violation of standards)
	8.9	Problems with bathing water quality
	8.10	Problems with irrigation water quality
	8.11	Problems with water quality for use in industrial production processes

	8.12	other
	8.13	Increased costs / economic losses
Freshwater ecosystems: habitats, plants and wildlife	9.1	Increased mortality of aquatic species (specify species (lati n term) and state whether a rare/endangered/protected species is conc erned in the description field)
	9.2	Increased species concentration near water
	9.3	Migration and concentration (loss of wildlife in some areas and too many in others)
	9.4	Increased populations of invasive (exotic) aquatic species
	9.5	Observation of adverse impacts on populations of rare/endangered (protected) riparian species
	9.6	Observation of adverse impacts on populations of rare/endangered (protected) species of wetlands
	9.7	Loss of biodiversity (decrease in species diversity)
	9.8	Violation of environmental /minimum flow threshold
	9.9	Drying up of shallow water areas, weed growth or algae bloom
	9.10	Drying up of perennial stream sections
	9.11	Drying up of lakes and reservoirs (which have a habitat function)
	9.12	(Mid-/Long-term) deterioration of wetlands
	9.13	Irreversible deterioration/loss of wetlands
	9.14	other
	9.15	Increased costs / economic losses
Terrestrial ecosystems: habitats, plants and wildlife	10.1	Increased species mortality (specify species (latin term) and state whether a rare / endangered / protected species is concerned
	10.2	Changes in species biology/ecology
	10.3	Loss of biodiversity (decrease in species diversity)
	10.4	Shift in species composition
	10.5	Reduced plant growth
	10.6	(Mid-/Long-term) deterioration of habitats
	10.7	Irreversible deterioration/loss of habitats
	10.8	Lack of feed / water for terrestrial wildlife
	10.9	Increased attacks of pests and diseases
	10.10	Increased contact of wild animals under stress (shortage / lack of feed and water) with humans/ human settlements
	10.11	other
	10.12	Increased costs / economic losses
Soil system	11.1	Drought-related erosion processes (loss of soil fertility)
	11.2	Structural damage to private property due to soil subsidence/shrinkage
	11.3	Structural damage to infrastructures due to soil subsidence/shrinkage
	11.4	other
	11.5	Increased costs / economic losses
Wildfires	12.1	Increased burned area
	12.2	Increased number of wildfires
	12.3	Increased severity of wildfires

	12.4	other
	12.5	Increased costs / economic losses
Air quality	13.1	Air quality pollution effects / problems (dust bowl effect, wildfires, substitution of hydropower production by fossil energy)
	13.2	other
	13.3	Increased costs / economic losses
Human health	14.1	Heat stress problems (if drought is associated with a heatwave)
	14.2	Increased respiratory ailments (heawave and air quality)
	14.3	Excess mortality during heat waves
	14.4	other
	14.5	Increased costs / economic losses
Conflicts	15.1	Water allocation conflicts-international
	15.2	Regional/local user conflicts
	15.3	other
	15.4	Increased costs / economic losses

References

Allen, Richard G., et al. "Crop evapotranspiration-Guidelines for computing crop water requirements-FAO Irrigation and drainage paper 56." *FAO, Rome* 300 (1998): 6541.

Abramowitz, Milton, and Irene A. Stegun. Handbook of mathematical functions. Vol. 1046. New York: Dover, 1965.

American Meteorological Society (AMS), 2" Statement on meteorological drought." Bull. Am. Meteorol. Soc. 85 (2004): 771–773

Dai, Aiguo. "Increasing drought under global warming in observations and models." *Nature Climate Change* 3.1 (2012): 52-58.

Déqué, Michel, et al. "The ARPEGE/IFS atmosphere model: a contribution to the French community climate modelling." *Climate Dynamics* 10.4-5 (1994): 249-266.

Déqué, M., and J. Ph Piedelievre. "High resolution climate simulation over Europe." *Climate dynamics* 11.6 (1995): 321-339.

Emerson, John D., and Judith Strenio. "Boxplots and batch comparison." *Understanding robust and exploratory data analysis* 58 (1983).

Fichefet, Thierry, and M. A. Maqueda. "Sensitivity of a global sea ice model to the treatment of ice thermodynamics and dynamics." *Journal of Geophysical Research: Oceans (1978–2012)* 102.C6 (1997): 12609-12646.

Goosse, Hugues, and Thierry Fichefet. "Importance of ice-ocean interactions for the global ocean circulation: A model study." *Journal of Geophysical Research: Oceans (1978–2012)* 104.C10 (1999): 23337-23355.

Guttman, Nathaniel B. "Accepting the standardized precipitation index: A calculation algorithm." (1999): 311-322.

IPCC "IPCC Technical Guidelines for Assessing Climate Change Impacts and Adaptations." Prepared by Working Group II [Carter, T.R., M.L. Parry, H. Harasawa, and S. Nishioka (eds.)] and WMO/UNEP. CGER-IO15-'94. University College -London, UK and Center

for Global Environmental Research, National Institute for Environmental Studies, Tsukuba, Japan (1994): 59 pp

IPCC-TGICA "General Guidelines on the Use of Scenario Data for Climate Impact and Adaptation Assessment. Version 2." Prepared by T.R. Carter on behalf of the Intergovernmental Panel on Climate Change, Task Group on Data and Scenario Support for Impact and Climate Assessment.) (2007)

Haddeland, Ingjerd, et al. "Multimodel estimate of the global terrestrial water balance: Setup and first results." *Journal of Hydrometeorology* 12.5 (2011): 869-884.

Hagemann, Stefan, et al. "Impact of a statistical bias correction on the projected hydrological changes obtained from three GCMs and two hydrology models." *Journal of Hydrometeorology* 12.4 (2011): 556-578.

Hannaford, J., et al. "The influence of decadal-scale variability on trends in long European streamflow records." *Hydrology and Earth System Sciences Discussions* 10.2 (2013): 1859-1896.

Hargreaves G.H. and Samani Z.A,. (1985) "Reference crop evapotranspiration from temperature." *Appl Engine Agric*. 1(2) (1985): 96–99

Hosking, J. R. M., "L-moments: Analysis and estimation of distributions using linear combinations or order statistics" J. R. Stat. Soc., Ser. B, 52, (1990): 105-124.

Hourdin, Frédéric, et al. "The LMDZ4 general circulation model: climate performance and sensitivity to parametrized physics with emphasis on tropical convection." *Climate Dynamics* 27.7-8 (2006): 787-813.

Jungclaus, J. H., et al. "Ocean circulation and tropical variability in the coupled model ECHAM5/MPI-OM." *Journal of climate* 19.16 (2006): 3952-3972.

Lehner, Bernhard, et al. "Estimating the impact of global change on flood and drought risks in Europe: a continental, integrated analysis." *Climatic Change* 75.3 (2006): 273-299.

Lloyd-Hughes, Benjamin, and Mark A. Saunders. "A drought climatology for Europe." *International Journal of climatology* 22.13 (2002): 1571-1592.

Madec, Gurvan, et al. "OPA 8.1 ocean general circulation model reference manual." *Note du Pôle de modélisation, Institut Pierre-Simon Laplace* 11 (1998).

Mavromatis, T., and P. D. Jones. "Evaluation of HadCM2 and direct use of daily GCM data in impact assessment studies." *Climatic Change* 41.3-4 (1999): 583-614.

McKee, Thomas B., Nolan J. Doesken, and John Kleist. "The relationship of drought frequency and duration to time scales." *Proceedings of the 8th Conference on Applied Climatology*. Vol. 17. No. 22. Boston, MA: American Meteorological Society, 1993.

Mishra, Ashok K., and Vijay P. Singh. "A review of drought concepts." *Journal of Hydrology* 391.1 (2010): 202-216.

Nakićenović et al. "Special Report on Emissions Scenarios: A Special Report of Working Group III of the Intergovernmental Panel on Climate Change" *Cambridge University Press*, (2000): 599 pp

Parry, Simon, et al. "Multi-year droughts in Europe: analysis of development and causes." *Hydrology Research* 43.5 (2012): 689-706.

Prudhomme, Christel, et al. "Hydrological droughts in the 21st century, hotspots and uncertainties from a global multimodel ensemble experiment." *Proceedings of the National Academy of Sciences* 111.9 (2013): 3262-3267.

Roeckner, Erich, et al. "The atmospheric general circulation model EHAM5. Part I: model description." (2003).

Royer, J-F., et al. "Simulation of climate changes during the 21st century including stratospheric ozone." *Comptes Rendus Geoscience* 334.3 (2002): 147-154.

Salas Mélia, D. "A global coupled sea ice–ocean model." *Ocean Modelling* 4.2 (2002): 137-172.

Sheffield, Justin, Eric F. Wood, and Michael L. Roderick. "Little change in global drought over the past 60 years." *Nature* 491.7424 (2012): 435-438.

Stagge, J.H , et al. " Standardized precipitation-evapotranspiration index (SPEI): Sensitivity to potential evapotranspiration model and parameters." *Proceedings of FRIEND-Water 2014* (2014)

Stagge, J.H , et al. " Candidate Distributions for Climatological Drought Indices (SPI and SPEI) " *International Journal of Climatology* (2014)

Stahl, K., et al. "Streamflow trends in Europe: evidence from a dataset of near-natural catchments." *Hydrology and Earth System Sciences Discussions* 7.4 (2010): 5769-5804.

Tallaksen, Lena M., and Henny AJ Van Lanen, eds. *Hydrological drought: processes and estimation methods for streamflow and groundwater*. Vol. 48. Elsevier, 2004.

Thornthwaite, Charles Warren. "An approach toward a rational classification of climate." *Geographical review* (1948): 55-94.

Vicente-Serrano, Sergio M., Santiago Beguería, and Juan I. López-Moreno. "A multiscalar drought index sensitive to global warming: the standardized precipitation evapotranspiration index." *Journal of Climate* 23.7 (2010): 1696-1718.

Viner, D., Hulme, M., 1997. "The Climate Impacts LINK Project: Applying Results of the Hadley Centre's Climate Change Experiments for Climate Change Impacts Assessment Report Prepared for the UK Department of the Environment Transport and the Regions" *Climatic Research Unit*. (1997): 16pp

Wanders, N., et al. "Future discharge drought across climate regions around the world modelled with a synthetic hydrological modelling approach forced by three General Circulation Models." *Nat. Hazards Earth Syst. Sci. Discuss.*, 1, (2013): 7701-7738

Wanders, N., Y. Wada, and H. A. J. Van Lanen. "Global hydrological droughts in the 21st century under a changing hydrological regime." *Future* 5 (2014): 649-681.

Weedon, G. P., et al. "Creation of the WATCH forcing data and its use to assess global and regional reference crop evaporation over land during the twentieth century." *Journal of Hydrometeorology* 12.5 (2011): 823-848.

Wilhite, Donald A., and Michael H. Glantz. "Understanding: the drought phenomenon: the role of definitions." *Water international* 10.3 (1985): 111-120.

World Meteorological Organization. " Standardized Precipitation Index User Guide" (M. Svoboda, M. Hayes and D. Wood). (WMO-No. 1090), (2012).